Check for updates

NANO · MICRO small
www.small-journal.com

Cross-Link-Dependent Ionogel-Based Triboelectric Nanogenerators with Slippery and Antireflective Properties

Yinghong Wu, Tyler J. Cuthbert, Yang Luo, Paul K. Chu, and Carlo Menon**

Given the ability to convert various ambient unused mechanical energies into useful electricity, triboelectric nanogenerators (TENGs) are gaining interest since their inception. Recently, ionogel-based TENGs (I-TENGs) have attracted increasing attention because of their excellent thermal stability and adjustable ionic conductivity. However, previous studies on ionogels mainly pursued the device performance or applications under harsh conditions, whereas few have investigated the structure–property relationships of components to performance. The results indicate that the ionogel formulation—composed of a crosslinking monomer with an ionic liquid—affects the conductivity of the ionogel by modulating the cross-link density. In addition, the ratio of cross-linker to ionic liquid is important to ensure the formation of efficient charge channels, yet increasing ionic liquid content delivers diminishing returns. The ionogels are then used in I-TENGs to harvest water droplet energy and the performance is correlated to the ionogels structure–property relationships. Improvement of the energy harvesting is further explored by the introduction of surface polymer brushes on I-TENGs via a facile and universal method, which enhances droplet sliding by means of ideal surface contact angle hysteresis and improves its anti-reflective properties by employing the I-TENG as a surface covering for solar cells.

1. Introduction

The growing popularity of smart electronics has triggered increasing demands for portable power sources. Triboelectric nanogenerators (TENGs) that are based on contact electrification and electrostatic induction are a promising energy harvesting technology that has the potential to generate electricity that is otherwise lost.[1,2] TENG can be produced from essentially any material opening up the capability of energy production in new areas. Electrodes can vary from classical rigid electrode materials such as metals[3] and semiconductors,[4] to soft electrodes such as conductive polymer films, hydrogels, or ionogels.[5] In addition, TENG is capable of converting many types of mechanical movements into electricity, such as human motion,[6] wind,[7] and water droplets.[8] Furthermore, the structural flexibility and simplistic working principle of TENGs allow it to be readily combined with other energy harvesting devices, such as piezoelectric nanogenerators,[9] electromagnetic generators,[10] and solar cells,[11] which increases the potential energy that can be harvested.

Ionic liquids (ILs) are molten salts that possess low volatility and can often be liquid at room temperature. The thermal stability and ionic conductivity of ILs are attractive properties for the replacement of water in hydrogels for many applications, which have given rise to IL-based gels (i.e., ionogels). In recent years, ionogels have been increasingly reported as soft conductors for TENGs by taking advantage of their adjustable conductivity, flexibility, transparency, as well as thermal stability.[12–16] Previously, ionogels have been reported as both the electrode and positively charged triboelectric layer;[12] recent examples of these ionogel-TENG (I-TENG) devices have shown use as stretch and tactile sensors and energy generating electronic skin.[13] Thus far, I-TENG studies have mainly focused on either improving the physical properties of ionogels such as stretchability,[14] or tailoring the properties of the ionogels for use in harsh conditions.[15] The conductivity of ionogels is an important parameter that can affect the ion transport and further charge induction and charge transfer of TENGs. How the relationship of ionogel components to conductivity and the translation to I-TENG device performance would be informative for advancing the performance of ionogel-based electronic device generally from a fundamental understanding perspective.

Water droplets possess mechanical energy that is prevalent, is a renewable source of energy, and thus far relatively underutilized. TENGs have been employed as water droplet harvesters previously, albeit with low output performance. To enhance the droplet harvesting efficiency, focus has been

Y. Wu, T. J. Cuthbert, C. Menon
Biomedical and Mobile Health Technology Lab
Department of Health Sciences and Technology
ETH Zürich
Lengghalde 5, Zürich 8008, Switzerland
E-mail: yinghong.wu@hest.ethz.ch; carlo.menon@hest.ethz.ch
Y. Luo, P. K. Chu
Department of Physics
City University of Hong Kong
Tat Chee Avenue, Kowloon, Hong Kong 999077, China
The ORCID identification number(s) for the author(s) of this article can be found under https://doi.org/10.1002/smll.202301381.

© 2023 The Authors. Small published by Wiley-VCH GmbH. This is an open access article under the terms of the Creative Commons Attribution-NonCommercial-NoDerivs License, which permits use and distribution in any medium, provided the original work is properly cited, the use is non-commercial and no modifications or adaptations are made.

DOI: 10.1002/smll.202301381

limited to increasing the hydrophobicity of the top surface.[17–20] These advancements have included employing patterned superhydrophobic fluorine-laser-induced graphene (F-LIG) layer on the TENG surface—imparting hydrophobicity to an otherwise hydrophilic substrate—resulting in a ten-times increase in device output.[17] The interfacial surface chemistry is known to be an important factor on improving TENG output, although other mechanisms of improvement may be possible and highly suited for combined energy harvesting.

Water droplet harvesting TENGs have been combined with solar cells to allow harvesting during both sunny and raining weather events. Presently, TENG cannot reach energy harvesting quantities of solar cells, but in combination provide avenues to achieve clean energy harvesting during different weather events. Previous research in using TENG as surface coverings for solar cells has focused on modifying the TENGs exposed surfaces to achieve both high hydrophobicity and good light absorption.[21–24] However, most enhancement methods employed are technically difficult/complicated to fabricate, or only applicable to limited sets of materials. A facile and universal surface enhancement method may improve the adoption of combining TENGs with solar cells and provide additional avenues to untapped renewable energy resources.

Herein, the relationship between cross-link density and ionogel ionic conductivity is explored and its relationship to I-TENG output is analyzed. The I-TENG is then used as a covering for a solar cell for power harvesting from water droplets. The enhancement of the I-TENG output is obtained by utilizing a surface polymer brush, which is synthesized using a universal vapor-phase polymerization procedure, imparting a slippery surface increasing the energy generation. Interestingly, the surface brush also provided an anti-reflective characteristic that was ideal for obtaining high solar cell performance.

2. Results and Discussion

The ionic liquid (IL) chosen was 1-butyl-3-methylimidazolium hexafluorophosphate ([BMIM]PF_6) and was synthesized from [BMIM]Cl through a salt metathesis reaction (**Figure 1**a, confirmed with ATR-FTIR in Figure S1, Supporting Information, and NMR in Figures S2–S4, Supporting Information). The [BMIM]PF_6 provided a hydrophobic, nonvolatile, and conductive room temperature liquid suitable for synthesizing an ionogel that can eliminate the presence of water in the network. The cross-linking monomer polyethylene glycol dimethacrylate (PEGDMA) was used as the sole polymerizable component since it can be obtained with various number average molecular weights (Mn) allowing the study of cross-link density. The cross-linking monomer was synthesized from the corresponding polyethylene glycol's (PEG with Mn of 400, 1500, 6000, 10 000, and 20 000 g moL^{-1}) as illustrated in Figure 1b and was confirmed with ^1H NMR (Figures S5–S9, Supporting Information).

As shown in Figure 1c, the ionogels were synthesized by photopolymerization; formulations consisted of PEGDMA, IL ([BMIM]PF_6), and photo-initiator phenylbis(2,4,6-trimethylbenzoyl)phosphine oxide (BAPO) under UV light (365 nm LEDs, see the Experimental Section for details). Monitoring the polymerization of acrylate-based formulations can be completed using ATR-FTIR spectroscopy analyzing the disappearance of the =C−H and C=C of the acrylate and normalizing to C−H bending at 2875 cm^{-1} of the PEG. As expected, the increasing peak intensities of the C=O stretch versus C−H bending match with the decreasing Mn of PEG cross-linking monomers (Figure 1d and Figure S10, Supporting Information). The disappearance of the methacrylate =C−H and C=C peaks and the shift of the C=O peak indicate essentially complete polymerization of the formulation. The other characteristic peaks are consistent with those shown in Figure S1 (Supporting Information), indicating the existence of [BMIM]PF_6 in the photopolymerized PEGDMA and the formation of ionogel. Therefore, our subsequent analysis focused on the effect of cross-link density and ionic liquid density on the ionogels conductivity. It is noted that the cross-link density is the number of polymerizable groups to the mass of cross-linker—the quantitative ratio of cross-links has been calculated. As shown in Figure 1e, when PEGDMA with higher initial Mn is used as the matrix of the gel, it has a lower cross-link density compared to that of a lower Mn PEGDMA.

It was found that the cross-link density of PEGDMA affected the conductivity of the ionogels for the same weight percent of IL (**Figure 2**a and Figure S11a, Supporting Information). Increasing the Mn of the cross-linker PEGDMA from 400 to 6000 increased the conductivity of the ionogels from 0.014 to 0.036 S m^{-1}. However, the conductivity decreased as PEGDMA Mn was increased to 10 000 and decreased further at an Mn of 20 000. Analogous results were obtained when changing the polymerizable group between methacrylate and acrylate (Figure S12, Supporting Information), leaving us with only the Mn of the cross-linker responsible for the change in ionic conductivity (Figure 2b). At a 1:1 ratio of PEGDMA:IL, the increase of ionic conductivity is directly related to the lower cross-link density and therefore increased charge mobility in the ionogel. The decrease in conductivity at higher PEGDMA Mn's was a result of incomplete swelling of the polymer matrix by the IL. Higher Mn requires greater ratios of IL to solvate the 10 000 and 20 000 PEGDMA, which is required to obtain a conductive network throughout the ionogel. The homogeneity of the ionogel can be analyzed using transmittance of UV–visible spectroscopy. The ability of the IL to solvate the PEGDMA is dependent on the weight ratio of the formulation (PEGDMA:IL) and the Mn of the PEGDMA. As the PEGDMA Mn is increased, the ability of the IL to solvate the PEGDMA is decreased, as shown in Figure 2a,c, where PEGDMA 10 000 and 20 000 had decreasing conductivity and transmittance.

By changing the ratio of PEGDMA:IL with a static PEGDMA Mn, we observed the same result whereby too little IL in the formulation would lead to decreased conductivity of the ionogel (Figure 2d and Figure S13, Supporting Information), which was accompanied by a decrease in transmittance through that gel (Figure 2e). Increasing the ratio of IL to PEGDMA increased the ionic conductivity and analogously eliminated any nonhomogeneity of the ionogel. For our formulations, there was a minimum amount of IL required to obtain a transparent film and below this ratio of components the amount of IL is not sufficient to solvate the PEGDMA. At a PEGDMA:IL ratio of 2:1, the ionogel was only possessed transmittance of ≈71% and had the lowest ionic conductivity of below 0.02 S m^{-1}. Increasing

© 2023 The Authors. Small published by Wiley-VCH GmbH

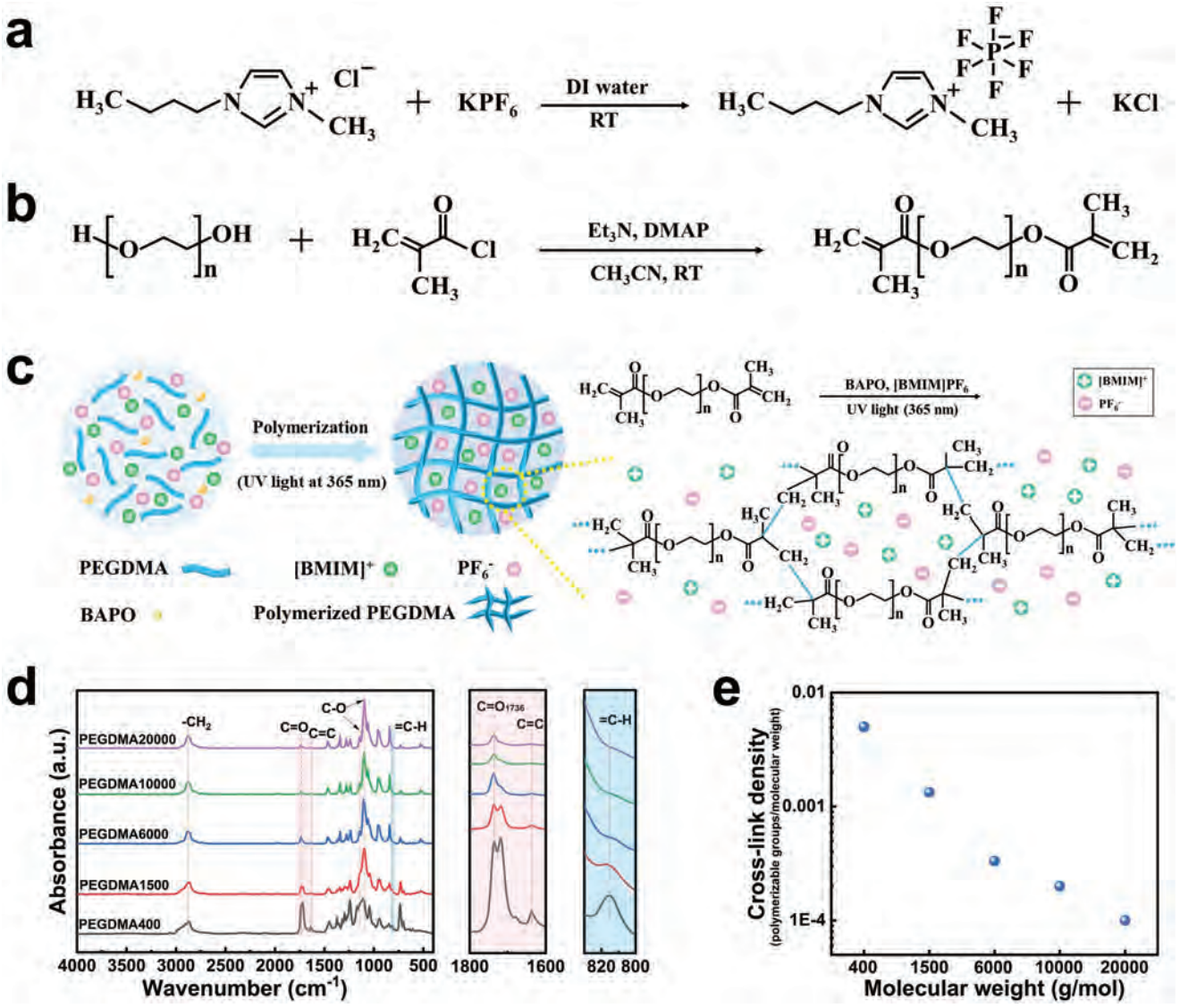

Figure 1. Synthesis and characterization of PEGDMA and its ionogels: a) synthesis reaction of $[BMIM]PF_6$, b) synthesis reaction of PEGDMA, c) schematic illustration of photopolymerization of PEGDMA with bond breaking and forming details, d) ATR-FTIR spectra of the synthesized PEGDMA, and e) cross-link density of PEGDMA with various average molecular weights.

to a ratio of PEGDMA:IL of 1:1 had a transmittance of ≈90% and an increase in ionic conductivity of up to 0.04 S m^{-1}. Increasing the ratio further with more IL resulted in completely transparent films with 100% transmittance, and an increasing ionic conductivity. The highest ratio of 1:8 PEGDMA:IL possessed the highest conductivity, although it was not eight times the conductivity of the 1:1 ratio ionogel. The reduction in ionic conductivity improvement likely because achieving complete charge channels (and fully swollen polymer networks) increases the conductivity more than increasing the amount of IL in the gel. Therefore, once ionic charge channels are formed and there is enough mobility in the viscous ionogel network (Figure 2f), the increase in conductivity across the gel is not greatly improved by further increasing the amount of IL in comparison to creating an efficient ionic network. Conversely, excess ILs in ionogels come at a cost of mechanical robustness (Figure 2g and Figure S14, see detailed discussion in the Supporting Information).

To elucidate if our ionogel findings in the above section affect the performance of the TENG, we then characterized the PEGDMA ionogel films with respect to cross-linking monomer Mn and IL weight percent as electrodes in TENGs for water droplet energy harvesting (**Figure 3**a). As shown in Figure 3b, the ionogel was sandwiched between two polydimethylsiloxane (PDMS) layers with two Ag tapes as the electrodes (one connected to the ionogel and the other to the top surface). When a single water droplet is dropped onto the inclined device, it slides down and off the surface and generates an electrical signal. The working mechanism of water droplet energy harvesting has been proposed previously[25,26] and the detailed discussion can be found in the Supporting Information (Figure S15, Supporting Information).

© 2023 The Authors. Small published by Wiley-VCH GmbH

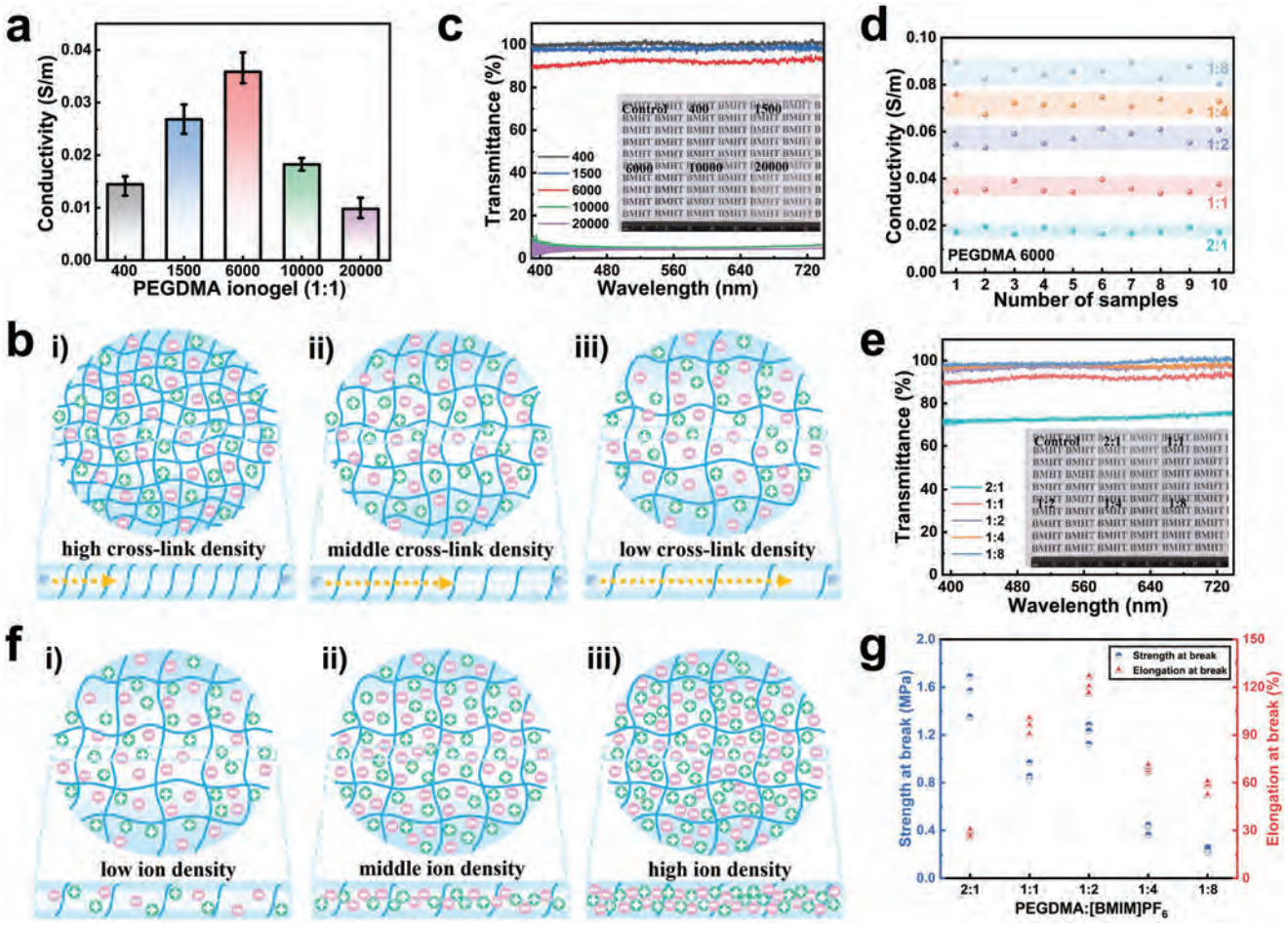

Figure 2. Interaction mechanism between cross linking and ion mobility and the impact on ionogels: a) dependence of the cross-link density on the conductivity of the ionogels, b) schematic diagram of ion mobility for different cross-link densities, c) effect of the cross-link density on the transmittance of the ionogels, d) dependence of the ion density on the conductivity of the ionogels, e) effect of the ion density on the transmittance of the ionogels, f) schematic diagram showing the formation of charge channel for various ion densities, and g) strength and elongation at break of ionogels with different PEGDMA:[BMIM]PF_6 ratios.

As shown in Figure 3c–e, the TENGs output matched our preliminary ionogel conductivity findings—we observed an increase in TENG output as the ionogel conductivity increased with decreasing cross-link density; PEGDMA 10 000 and 20 000 decreased in output, which meant that electrode ionic conductivity has a direct relationship with the output of the TENGs employing ionogels. The TENG output increase when using higher conductivity ionogels was reasoned to aid in charge induction and result in faster charge transfer. The output of the TENG device when the ratio of IL was increased from 2:1 to 1:8 PEGDMA:IL increased in both voltage and current (Figure S16, Supporting Information, and Figure 3f), with the highest of both occurring in the 1:8 PEGDMA:IL sample. The increase of voltage and current do not increase linearly with the increases of PEGDMA:IL. These data follow the same trend as the ionic conductivity in the optimization of the ionogel, indicating that for each Mn of PEGDMA there is likely an ideal ratio of cross-linking monomer to IL; increasing the IL weight percent beyond this ideal ratio will lead to a diminishing return in conductivity and reduce the mechanical properties such that they may not be robust enough for the intended use (Figure 2g and Figure S14, Supporting Information). Therefore, the formulation PEGDMA 6000:[BMIM]PF_6 with a ratio of 1:2 was therefore chosen for the subsequent investigation.

To assess the practical use of the electricity generated by water droplets energy harvesting, the PEGDMA 6000-1:2 device was connected to a circuit consisting of a rectifier and external loads including resistors and LEDs as shown in Figure S17 (Supporting Information). As the load resistance was raised from 100 to 200 MΩ, the current decreased and the voltage increased according to the Ohm's law. Thus, the generated power ($P_R = I_R{*}V_R$, Figure 3h) increased initially and then declined when the resistance was increased. The maximum power reached 115.2 μW for a load resistance of 2 MΩ. When further connecting the circuit to LEDs, it was observed in the Video S1 (Supporting Information) and the inset of Figure 3h that a single droplet moving across the device can light up 18 LEDs connected in series.

To improve the TENG output for water droplet energy harvesting, previous works focused on increasing the hydrophobicity of the device by physical modification or chemical functionalization.[17,20,27] An alternative method that we hypothesized

© 2023 The Authors. Small published by Wiley-VCH GmbH

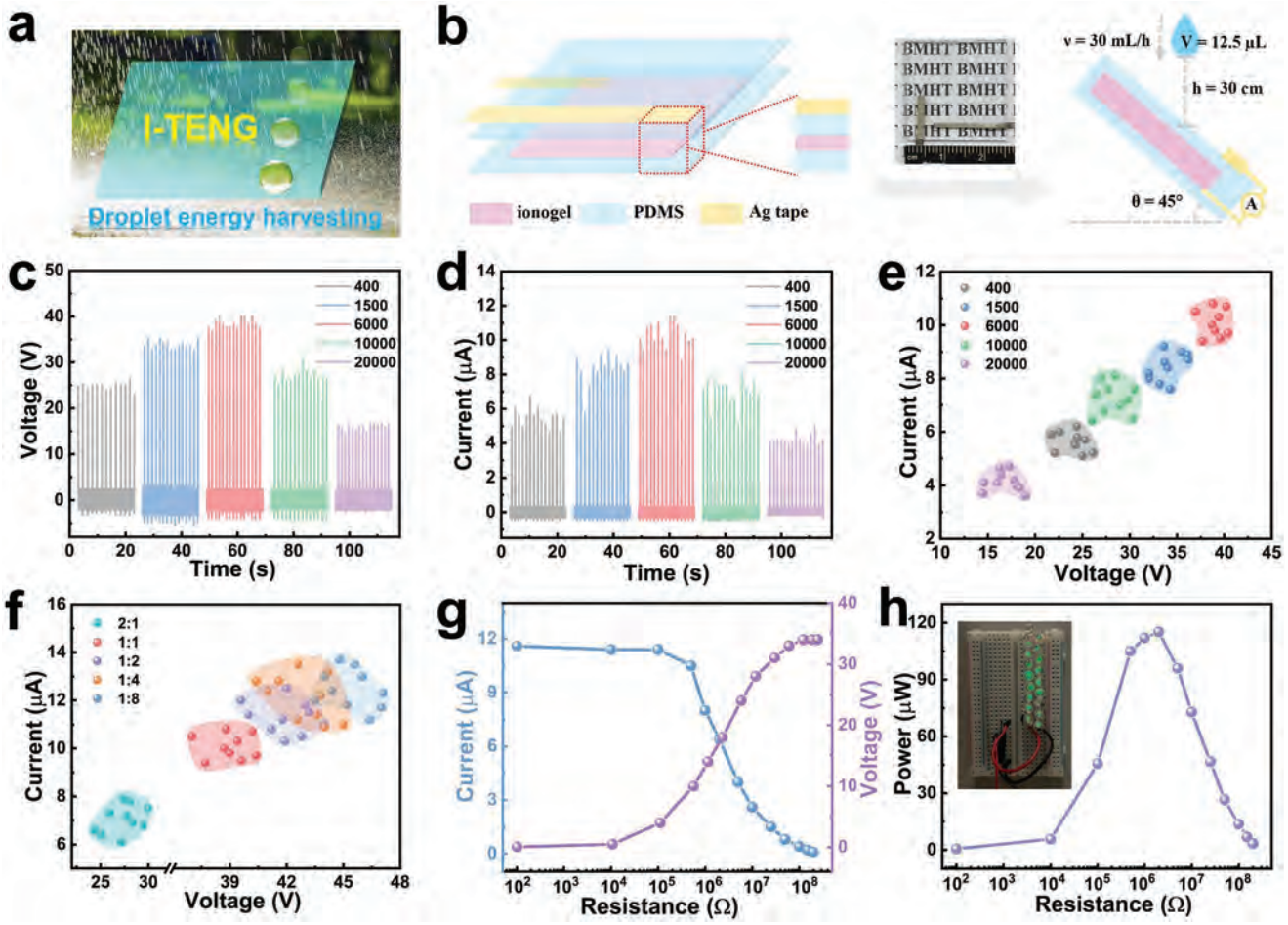

Figure 3. Demonstration of I-TENGs for droplet energy harvesting: a) schematic diagram of TENGs harvesting droplets energy, b) schematic diagram and photograph of a typical I-TENG, and the measurement conditions for water droplet energy harvesting, c–e) effect of the cross-link density on the device output, f) effect of the ion density on the device output, g) dependence of the load resistance on the voltage and current, and h) dependence of the load resistance on the power, with the inset is showing 18 green LEDs lit up by one single droplet.

would improve the output of the TENG is to impart greater water droplet sliding efficiency rather than simply a more hydrophobic surface. Therefore, we decided to induce a type of slippery surface by employing PDMS brushes fabricated with vapor-phase polymerization directly on the surface—a synthetic strategy that is relatively simple and universal if −OH are available. Inspired by previous studies,[28,29] when the material/device was pretreated with an air plasma—to create surface −OH functionality—the vapor-phase polymerization of PDMS was possible with dichlorodimethylsilane (DCDMS) and water vapor in a closed container as shown in **Figure 4**a. Consequently, many PDMS brushes will form and grow on the material surface as illustrated in Figure 4b. The effect of the PDMS brush on water droplet surface sliding resulted in an increase in water droplet sliding across the surface when at a nonzero angle (Video S2, Supporting Information). Water droplets were static on the untreated PDMS surface, whereas the droplet slid to the end of the PDMS/PDMS brushes surface in a few seconds at an angle of 45°. PDMS brushes act as lubricating layers and provide access to hydrophobic slippery surfaces through low contact angle hysteresis, which is a function of high mobility of the siloxane brushes.[30] Further investigation of the static water contact angles of these two surfaces reveals no obvious difference (i.e., on a flat surface, Figure S18, Supporting Information), which comes from same intrinsic chemical components of PDMS and PDMS brushes. SEM (Figure S19, Supporting Information) and AFM (Figure S20, Supporting Information) images without or with PDMS brushes were further provided and discussed (see details in Supporting information). As shown in Figure 4c–e, the increase in water droplet sliding resulted in the average voltage and current increasing from 42 V and 11.3 μA to 55.4 V and 14.6 μA. Improving the "slipperiness" of the TENGs surface can force the water droplet to move faster along the surface, have a faster charge induction and accumulation, and thus generate a sharper electrical signal.

To assess the performance of the PI-TENGs in real use-case scenarios, rainwater collected in Zurich, Switzerland was tested for harvesting droplet energy. As shown in Figure S21 (Supporting Information) and Figure 4f, replacement of distilled water with rainwater produces a higher voltage and current. It was found that the highly increased conductivity of the rainwater (Figure S22, Supporting Information) was the main

© 2023 The Authors. Small published by Wiley-VCH GmbH

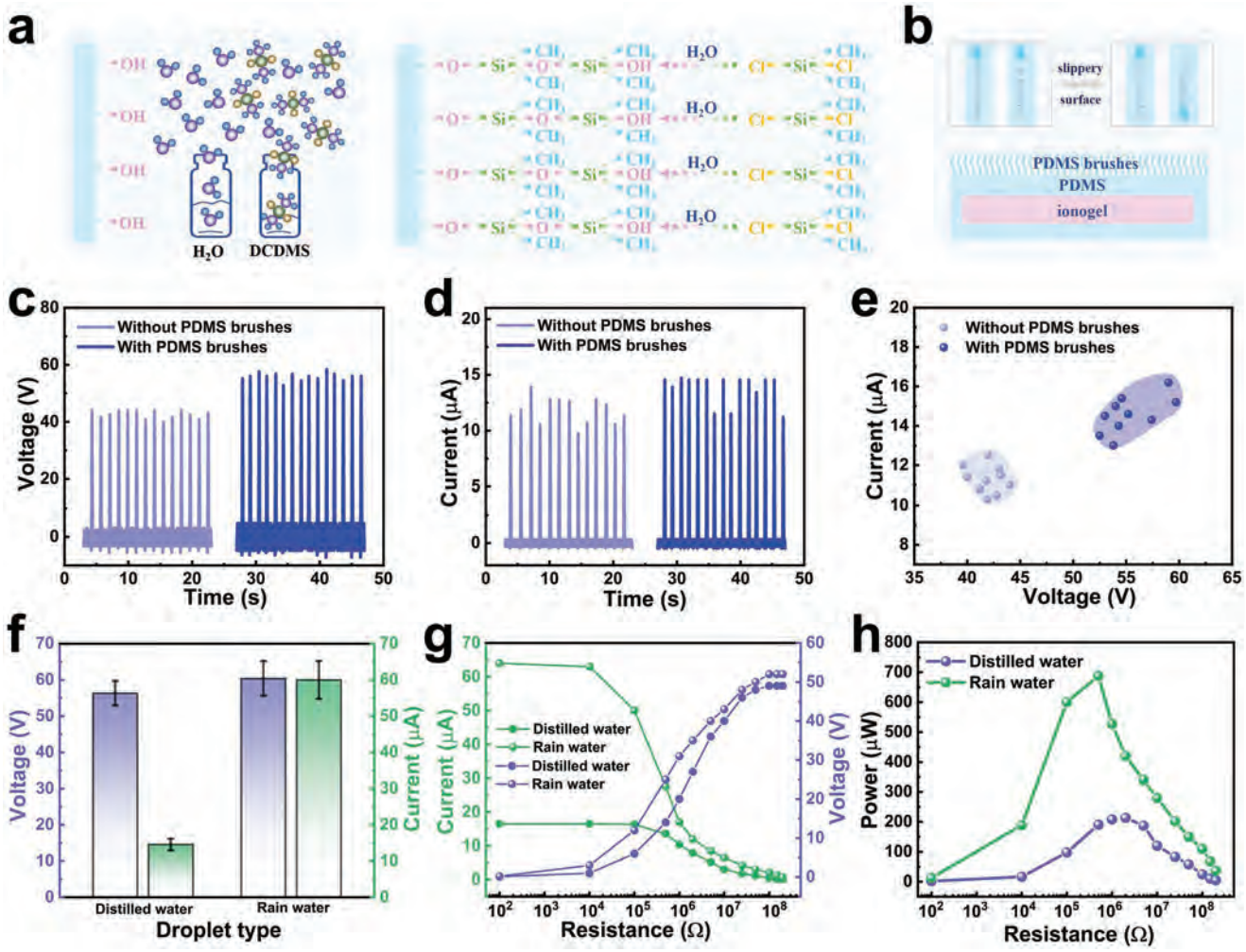

Figure 4. Introduction of PDMS brushes for the output enhancement of I-TENGs: a) schematic showing the synthesis of the PDMS brushes, b) schematic diagram of the typical PI-TENG and sliding comparison of the surfaces with or without PDMS brushes, c–e) effect of PDMS brushes on the device output, f) effect of distilled water and rainwater (Swiss) droplets on the device output, g) dependence of the load resistance on the voltage and current for distilled water or rainwater droplets, and h) dependence of the load resistance on the power for distilled water or rainwater droplets.

factor contributing to the current increase, as the higher conductivity of rainwater gave rise to faster directional transfer of charges and thus sharper signals.[25,26] When connecting the device to the external load resistance, the difference in current between distilled water and rainwater (Figure 4g) resulted in apparent power difference (Figure 4h). The maximum power achieved by rainwater was 688 μW, which was 3.2 times that of distilled water. As shown in Table S1 (Supporting Information), the developed devices in the work showed high output performance compared with reported TENGs in droplet energy harvesting.

As shown in Figure S23 (Supporting Information), I-TENGs with or without PDMS brushes both had a high transmittance of >95% in the visible light range. With our understanding of how to improve power output by creating a slippery and transparent I-TENG, we decided on an appropriate application as a solar cell coating. The I-TENG covering possessed an antireflective property, which was ideal for covering a solar cell (**Figure 5**a). As shown in Figure 5b,c and Table S2 (Supporting Information), the silicon solar cell covered with our I-TENG exhibited an open-circuit voltage (V_{OC}) of 3.45 V, short-circuit current density (J_{SC}) of 5.88 mA cm^{-2}, and power conversion efficiency (PCE) of 17.23%. These characteristics were similar to those of bare solar cells, indicating the highly transparent I-TENG did not impact the performance of solar cells. When the PI-TENG was covered on the solar cell, J_{SC} increased from 5.81 to 6.13 mA cm^{-2} and PCE from 17.14% to 18.24%. The 1.1% increase of PCE stems from more light accessing the solar cell through the PDMS brushes, as these brushes on the surface result in greater refraction and diffraction rather than reflection.[31,32] As shown in Table S3 (Supporting Information), the PCE increase caused by the PI-TENG covering was high compared with reported works combining TENGs and solar cells. The fill factor (Figure 5c) was barely affected by the covered I-TENG and PI-TENG. The concept of PDMS brushes can be extended to common materials (such as metals, polymers, etc.), thus constituting a mild and universal strategy to enhance the properties of both TENGs and solar cells.

© 2023 The Authors. Small published by Wiley-VCH GmbH

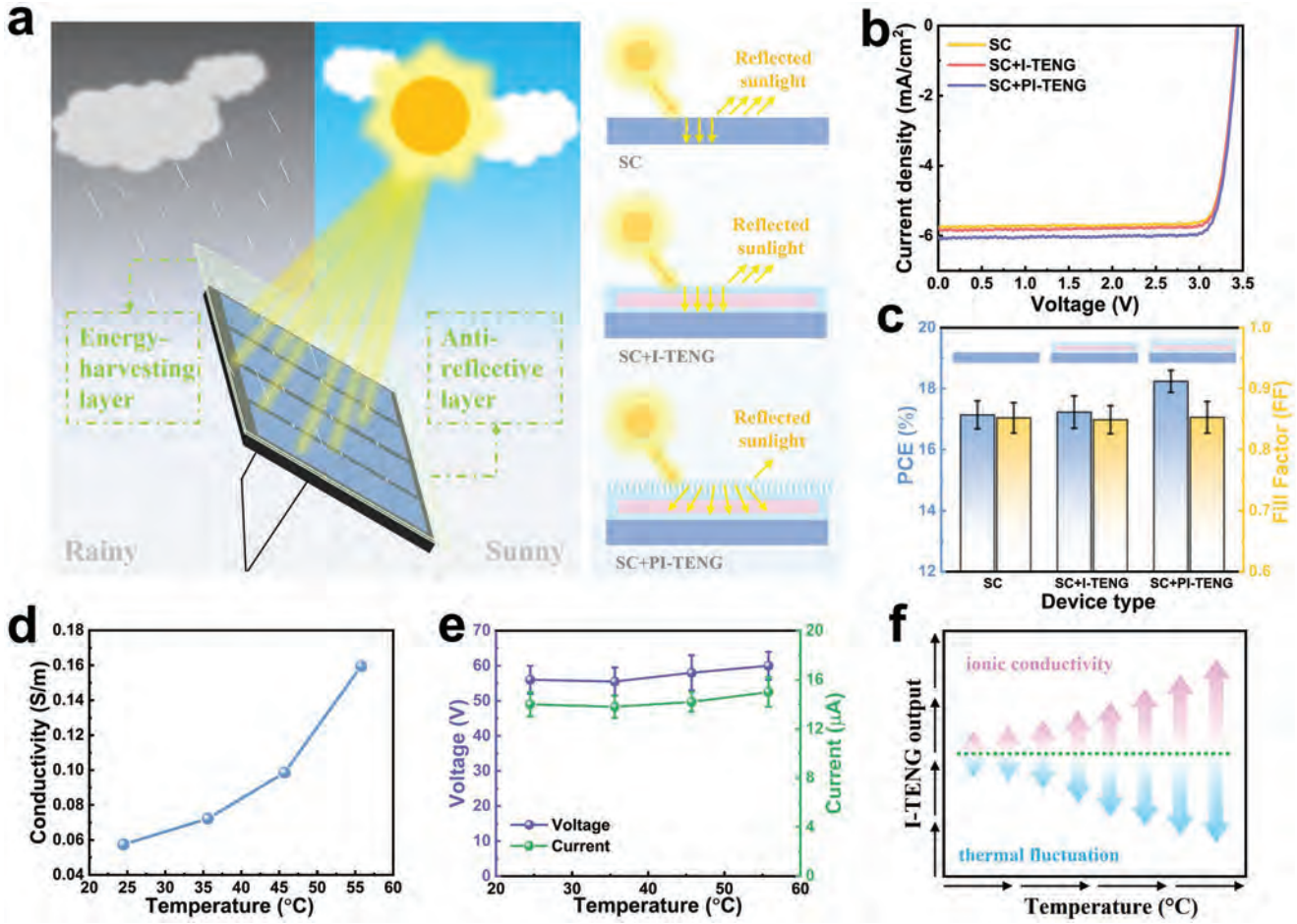

Figure 5. Introduction of PDMS brushes on the performance improvement of solar cells: a) schematic diagram of the PI-TENGs working as both energy harvesting and anti-reflective layers, and the enhancement mechanism caused by anti-reflection, b) *J–V* curves of the bare SC, SC+I-TENG, and SC+PI-TENG, c) PCE and FF comparison between the bare SC, SC+I-TENG, and SC+PI-TENG, d) dependence of temperature on the conductivity of ionogels, e) dependence of the temperature on the output of PI-TENGs, and f) schematic diagram of the two main factors affecting the temperature-output stability of the devices.

Other previous reports have focused on the simultaneous harvesting of droplet and solar energy.[21,23,33] However, in reality, most of the time the solar cell or the droplet harvesting will be functioning separately at different times. Thus, it was important for us to investigate if there was any influence of the solar cell on the TENG. We expect that in typical use a solar cell is exposed to increased temperatures as it is meant to be in direct sunlight. It is known that, for common TENGs, a higher temperature decreases the device output because of the thermal fluctuation and electron thermionic emission.[34,35] On the other hand, a higher temperature increases the conductivity of ionogels because of the reduced viscosity and increased ion mobility. As shown in Figure 5d, when the temperature increased from 25 to 56 °C, the conductivity of the ionogel increased from 0.057 to 0.16 S m^{-1}, and thus the device output was expected to increase. However, the results in Figure 5e indicate that both the voltage and current exhibit no appreciable change in the temperature range of 25–56 °C, which is consistent with previous reports using ionogels as electrodes.[36,37] Therefore, for I-TENG systems, there are two opposite factors balancing the temperature effect as shown in Figure 5f. On one hand, the temperature increase leads to the conductivity increase and thus the output enhancement. On the other hand, the temperature increase also produces thermal fluctuation or electron thermionic emission to decrease the output. The two competing factors likely increase with the increase of temperature, resulting in a stable device output. Therefore, the temperature rise from sun exposure does not affect the operation of the covered I-TENGs, which is another advantage of this work compared to common reported TENGs combining with solar cells.

3. Conclusion

The impacts of cross-link density of the monomer and ion density of the ionic liquid on the conductivity of ionogels were investigated systematically to elucidate the structure–function relationship to the TENG output. Owing to the faster ion mobility with the lower cross-link density, the ionogels with a PEGDMA synthesized from PEG 6000 possessed the best ionic conductivity within our formulation matrix. We found

© 2023 The Authors. Small published by Wiley-VCH GmbH

a minimum ionic liquid density was required in the gel to form a complete charge channel. As a demonstration, the ionogels were employed as electrodes of droplet-TENGs to harvest energy from rainfall. The growth of PDMS brushes on I-TENGs not only enhanced the device output because of faster water droplet sliding, but also improved the performance of solar cells by serving as an anti-reflective layer. This study reveals insights about the relation between the cross-link density and ion mobility to ionic conductivity, which can be used to optimize device and material performance for future ionogel employment in TENGs and devices requiring ionic conductors. The proposed PDMS brushes strategy has the potential to be extended to all types of TENGs and solar cells to enhance their performance in electronic applications.

Supporting Information

Supporting Information is available from the Wiley Online Library or from the author.

Acknowledgements

This work was supported by the City University of Hong Kong Donation Research Grant (DON-RMG No. 9229021) and City University of Hong Kong Strategic Research Grant (SRG No. 7005505). The authors would like to thank Mr. Yi-Hsuan Wu for his assistance in the solar simulator operation and Dr. Alexander V. Shokurov for his guidance in the EIS measurement.

Open access funding provided by Eidgenossische Technische Hochschule Zurich.

Conflict of Interest

The authors declare no conflict of interest.

Data Availability Statement

The data that support the findings of this study are available from the corresponding author upon reasonable request.

Keywords

cross-linking, ionogel, polymer brushes, rainwater, solar energy, triboelectric nanogenerators

Received: February 15, 2023
Published online: March 14, 2023

[1] J. Wang, C. Wu, Y. Dai, Z. Zhao, A. Wang, T. Zhang, Z. L. Wang, *Nat. Commun.* **2017**, *8*, 88.
[2] F.-R. Fan, Z.-Q. Tian, Z. L. Wang, *Nano Energy* **2012**, *1*, 328.
[3] Y.-M. Jo, Y. K. Jo, J.-H. Lee, H. W. Jang, I.-S. Hwang, D. J. Yoo, *Adv. Mater.* **2022**, 2206842.
[4] S. Chun, I. Y. Choi, W. Son, J. Jung, S. Lee, H. S. Kim, C. Pang, W. Park, J. K. Kim, *ACS Energy Lett.* **2019**, *4*, 1748.
[5] Y. Wu, Y. Luo, T. J. Cuthbert, A. V. Shokurov, P. K. Chu, S.-P. Feng, C. Menon, *Adv. Sci.* **2022**, *9*, 2106008.
[6] Y. Song, J. Min, Y. Yu, H. Wang, Y. Yang, H. Zhang, W. Gao, *Sci. Adv.* **2020**, *6*, eaay9842.
[7] L. He, C. Zhang, B. Zhang, O. Yang, W. Yuan, L. Zhou, Z. Zhao, Z. Wu, J. Wang, Z. L. Wang, *ACS Nano* **2022**, *16*, 6244.
[8] J. Nauruzbayeva, Z. Sun, A. Gallo, M. Ibrahim, J. C. Santamarina, H. Mishra, *Nat. Commun.* **2020**, *11*, 5285.
[9] Y. Wu, J. Qu, W. A. Daoud, L. Wang, T. Qi, *J. Mater. Chem. A* **2019**, *7*, 13347.
[10] S. M. S. Rana, M. Salauddin, M. Sharifuzzaman, S. H. Lee, Y. D. Shin, H. Song, S. H. Jeong, T. Bhatta, K. Shrestha, J. Y. Park, *Adv. Energy Mater.* **2022**, *12*, 2202238.
[11] J. Chen, Y. Huang, N. Zhang, H. Zou, R. Liu, C. Tao, X. Fan, Z. L. Wang, *Nat. Energy* **2016**, *1*, 16138.
[12] G. Zhao, Y. Zhang, N. Shi, Z. Liu, X. Zhang, M. Wu, C. Pan, H. Liu, L. Li, Z. L. Wang, *Nano Energy* **2019**, *59*, 302.
[13] B. Yiming, X. Guo, N. Ali, N. Zhang, X. Zhang, Z. Han, Y. Lu, Z. Wu, X. Fan, Z. Jia, S. Qu, *Adv. Funct. Mater.* **2021**, *31*, 2102773.
[14] S. Hao, T. Li, X. Yang, H. Song, *ACS Appl. Mater. Interfaces* **2022**, *14*, 2029.
[15] X. Zhong, P. Sun, R. Wei, H. Dong, S. Jiang, *J. Mater. Chem. A* **2022**, *10*, 15080.
[16] C. Dang, C. Shao, H. Liu, Y. Chen, H. Qi, *Nano Energy* **2021**, *90*, 106619.
[17] Y. Chen, B. Xie, J. Long, Y. Kuang, X. Chen, M. Hou, J. Gao, S. Zhou, B. Fan, Y. He, Y.-T. Zhang, C.-P. Wong, Z. Wang, N. Zhao, *Adv. Mater.* **2021**, *33*, 2104290.
[18] Q. Zhang, C. Jiang, X. Li, S. Dai, Y. Ying, J. Ping, *ACS Nano* **2021**, *15*, 12314.
[19] M. Sun, Q. Lu, Z. L. Wang, B. Huang, *Nat. Commun.* **2021**, *12*, 1752.
[20] M. A. M. Hasan, T. Zhang, H. Wu, Y. Yang, *Adv. Energy Mater.* **2022**, *12*, 2201383.
[21] Y. Zheng, T. Liu, J. Wu, T. Xu, X. Wang, X. Han, H. Cui, X. Xu, C. Pan, X. Li, *Adv. Mater.* **2022**, *34*, 2202238.
[22] Y. Liu, N. Sun, J. Liu, Z. Wen, X. Sun, S.-T. Lee, B. Sun, *ACS Nano* **2018**, *12*, 2893.
[23] D. Yoo, S.-C. Park, S. Lee, J.-Y. Sim, I. Song, D. Choi, H. Lim, D. S. Kim, *Nano Energy* **2019**, *57*, 424.
[24] Y. Wu, Y. Mu, Y. Luo, C. Menon, Z. Zhou, P. K. Chu, S.-P. Feng, *Adv. Funct. Mater.* **2022**, *32*, 2110859.
[25] W. Xu, H. Zheng, Y. Liu, X. Zhou, C. Zhang, Y. Song, X. Deng, M. Leung, Z. Yang, R. X. Xu, Z. L. Wang, X. C. Zeng, Z. Wang, *Nature* **2020**, *578*, 392.
[26] Q. Zhang, Y. Li, H. Cai, M. Yao, H. Zhang, L. Guo, Z. Lv, M. Li, X. Lu, C. Ren, P. Zhang, Y. Zhang, X. Shi, G. Ding, J. Yao, Z. Yang, Z. L. Wang, *Adv. Mater.* **2021**, *33*, 2105761.
[27] C. Ye, D. Liu, X. Peng, Y. Jiang, R. Cheng, C. Ning, F. Sheng, Y. Zhang, K. Dong, Z. L. Wang, *ACS Nano* **2021**, *15*, 18172.
[28] S. Shabanian, B. Khatir, A. Nisar, K. Golovin, *Nat. Sustain.* **2020**, *3*, 1059.
[29] J. Liu, Y. Sun, X. Zhou, X. Li, M. Kappl, W. Steffen, H.-J. Butt, *Adv. Mater.* **2021**, *33*, 2100237.
[30] S. Wooh, D. Vollmer, *Angew. Chem., Int. Ed.* **2016**, *55*, 6822.
[31] Z. Ren, Q. Zheng, H. Wang, H. Guo, L. Miao, J. Wan, C. Xu, S. Cheng, H. Zhang, *Nano Energy* **2020**, *67*, 104243.
[32] B. Dudem, J. W. Jung, J. S. Yu, *J. Mater. Chem. A* **2018**, *6*, 14769.
[33] L. Xu, L. Xu, J. Luo, Y. Yan, B.-E. Jia, X. Yang, Y. Gao, Z. L. Wang, *Adv. Energy Mater.* **2020**, *10*, 2001669.
[34] X. Wen, Y. Su, Y. Yang, H. Zhang, Z. L. Wang, *Nano Energy* **2014**, *4*, 150.
[35] C. Xu, A. C. Wang, H. Zou, B. Zhang, C. Zhang, Y. Zi, L. Pan, P. Wang, P. Feng, Z. Lin, Z. L. Wang, *Adv. Mater.* **2018**, *30*, 1803968.
[36] L. Sun, S. Chen, Y. Guo, J. Song, L. Zhang, L. Xiao, Q. Guan, Z. You, *Nano Energy* **2019**, *63*, 103847.
[37] W. Liao, X. Liu, Y. Li, X. Xu, J. Jiang, S. Lu, D. Bao, Z. Wen, X. Sun, *Nano Res.* **2022**, *15*, 2060.

© 2023 The Authors. Small published by Wiley-VCH GmbH

NANO MICRO small

Supporting Information

for *Small,* DOI: 10.1002/smll.202301381

Cross-Link-Dependent Ionogel-Based Triboelectric Nanogenerators with Slippery and Antireflective Properties

Yinghong Wu, Tyler J. Cuthbert, Yang Luo, Paul K. Chu, and Carlo Menon**

Cross-Link-Dependent Ionogel-Based Triboelectric Nanogenerators with Slippery and Anti-Reflective Properties

Yinghong Wu, Tyler J. Cuthbert, Yang Luo, Paul K. Chu, and Carlo Menon**

Dr. Y. Wu, Dr. T. J. Cuthbert, Prof. C. Menon
Biomedical and Mobile Health Technology Lab, Department of Health Sciences and Technology, ETH Zurich, Zurich, Switzerland.
E-mail: yinghong.wu@hest.ethz.ch, carlo.menon@hest.ethz.ch

Dr. Y. Luo and Prof. P. K. Chu
Department of Physics, City University of Hong Kong, Hong Kong, China.

1. Experimental section

Materials: All chemicals including 1-putyl-3-methylimidazolium chloride ([BMIM]Cl), potassium hexafluorophosphate (KPF_6), polyethylene glycol (PEG with different average Mn), methacryloyl chloride (MAC), triethylamine (Et_3N), dimethyl aminopyridine (DMAP), hydrochloric acid (HCl), dichloromethane (DCM), sodium carbonate (Na_2CO_3), sodium chloride (NaCl), sodium sulfate (Na_2SO_4), phenylbis(2,4,6-trimethylbenzoyl)phosphine oxide (BAPO), and dichlorodimethylsilane (DCDMS) were purchased from Sigma-Aldrich.

Synthesis of 1-putyl-3-methylimidazolium hexafluorophosphate ([BMIM]PF_6): 2M [BMIM][Cl] and 2M potassium hexafluorophosphate were mixed with DI water and stirred for 6 h. After two immiscible phases were formed, the aqueous and organic phases were separated from each other with a separating funnel. The organic phase was washed with water until the pH did not change, and volatiles were then removed in vacuo to give [BMIM]PF_6 as a room temperature ionic liquid.

Synthesis of PEGDMA: Polyethylene glycol was dissolved in acetonitrile and stirred at

room temperature under an N_2 atmosphere. Methacryloyl chloride (excess) was added to the mixture and stirred for 5 min. Et_3N was added slowly to ensure that the solution remained at room temperature. Dimethylaminopyridine was then added, and the solution stirred for 16-166 h. Volatiles were then removed in vacuo at 35 °C and 5 mbar. $HCl_{(aq)}$ (0.1 M) was then added to the resulting product and stirred for 10 min. Liquid–liquid extraction of the product was completed with dichloromethane (5x20 mL), which was then washed with 1M $Na_2CO_{3(aq)}$ and a brine solution (conc NaCl) each 5x. To the organic layer, solid Na_2SO_4 was added until a clear organic fraction was obtained, gravity filtered to obtain the organic layer, and volatiles were removed in vacuo, obtaining PEGDMA as an oily liquid or waxy solid, which was stored at -20 °C.

Table of PEDGMA synthesis component ratios

PEG Mn	PEG (g)	MAC (mL)	Et_3N (g)	Solvent [mL]	Reaction Duration (h)	Conversion to methacrylate. (%)
400	2 g	1.07 mL	5.06 g	50 mL	16 h	100%
1000	2 g	0.43 mL	2.02 g	50 mL	60 h	73%
6000	2 g	0.07 mL	0.34 g	50 mL	120 h	92%
10,000	2 g	0.04 mL	0.20 g	50 mL	133 h	61%
20,000	2 g	0.02 mL	0.10 g	50 mL	166 h	64%

Synthesis of ionogels: phenylbis(2,4,6-trimethylbenzoyl)phosphine oxide (1 wt% with respect to PEGDMA) as the photoinitiator was dissolved in the PEGDMA solution (at RT or 60 °C). [BMIM]PF_6 (2:1-1:8 to PEGDMA) was added to the mixture to form the ionic gel precursor formulation. After dropping the formulation onto a glass plate (50-100 µL), the gel precursor was covered by another glass plate and illuminated with UV light (365 nm) for 5 min

to obtain a transparent and uniform ionogel film.

Synthesis of the PDMS brushes: The substrate to be coated was treated by an air plasma (FEMTO, a low-pressure plasma system with an O_2 flow rate of 5 sccm) for 3 min and put into a glass container. Water and dichlorodimethylsilane (0.5–1 mL each, in separate glass vials) were combined in a closed glass desiccator for 30 min with the substrate, and subsequently washed thoroughly with isopropanol to remove any non-covalently attached byproducts.

Fabrication of the I-TENG: The PDMS mixture (polydimethylsiloxane, 10:1, Sylgard 184, 200-300 μL) was spread on a flat substrate and rotated on a spin-coater at 1500 rpm for 20 s. After drying at 80 °C for 2 h, the transparent and smooth PDMS film was removed from the substrate. The I-TENG consisted of a sandwiched structure (PDMS-ionogel-PDMS). For the output measurement, Ag tape was connected to the ionogel and another one to the edge of the top surface. The schematic diagram and photograph of the typical device are depicted in Figure 3b.

Characterization and measurement: The functional group of the samples were analyzed by an Attenuated Total Reflectance (ATR) Fourier transform infrared spectrometer (FTIR, ALPHA, Bruker). The conversion of PEG to PEGDMA was analyzed by a ^{1}H Nuclear Magnetic Resonance Spectroscopy (^{1}H NMR, Bruker 400 MHz). The transmittance of the samples was monitored by a fiber optic spectroscopy setup using a light source (SLS201L/M, ThorLabs), visible light spectrometer (CCS100/M, Thorlabs), optical fibers, and collimating lenses. The conductivity of the samples was evaluated by a potentiostat/galvanostat with integrated impedance analyzer (μStat-i 400, Metrohm DropSens). The mechanical properties of the samples were conducted by an electrodynamic test instrument (Electropuls E3000, Instron). The water contact angle of the samples was measured by an optical tensiometer (Theta Lite, Biolin Scientific). The surface morphology of the samples was measured by a scanning electron microscope (SEM, SU5000, HITACHI) and an atomic force microscopy (AFM,

FastScan, Bruker). The dripping rate of the droplets was controlled by a syringe pump (SKU300, InfusionONE). The TENG output was measured by an oscilloscope (MDO34, Tektronix) with a high voltage probe (PR1050D, RIGOL) and a low-noise current preamplifier (SR570, Stanford Research Systems). The droplet experiments were performed using the following parameters: volume = 12.5 μL, height = 30 cm, dripping rate = 30 mL/h, sliding angle = 45°, and water type = distilled water or rainwater. The I-V curve of the solar cell was collected by a VoltaLab 40 potentiostat with a Xe arc lamp solar simulator (LOT-Oriel) with a standard AM 1.5G light illumination (100 mW/cm^2).

2. Supplemental data

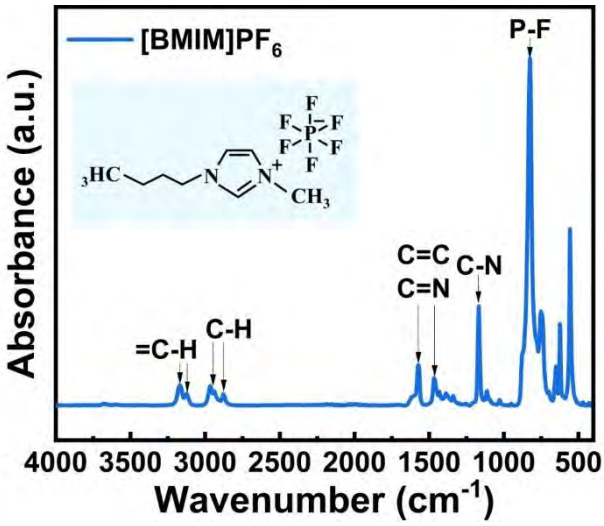

Figure S1. ATR-FTIR spectrum of [BMIM]PF_6, inset is the molecular structure of [BMIM]PF_6.

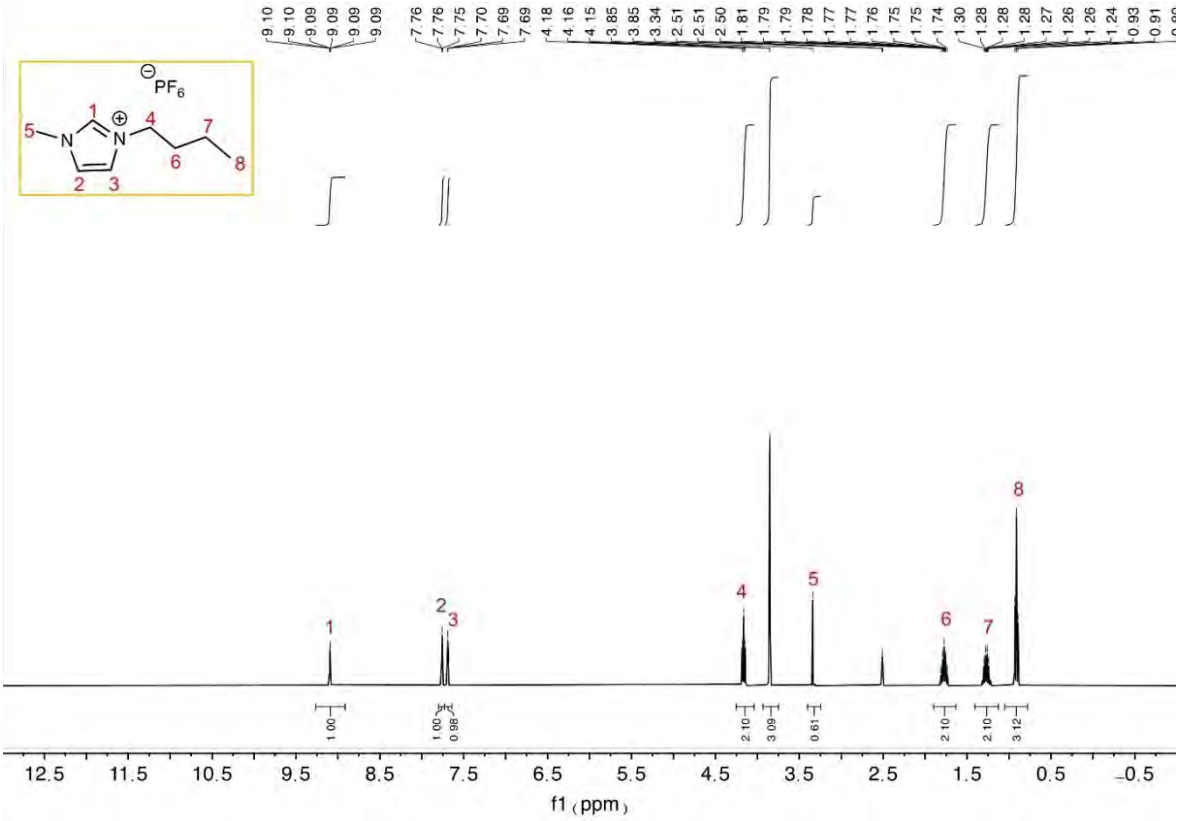

Figure S2. 1H NMR of [BMIM]PF_6.

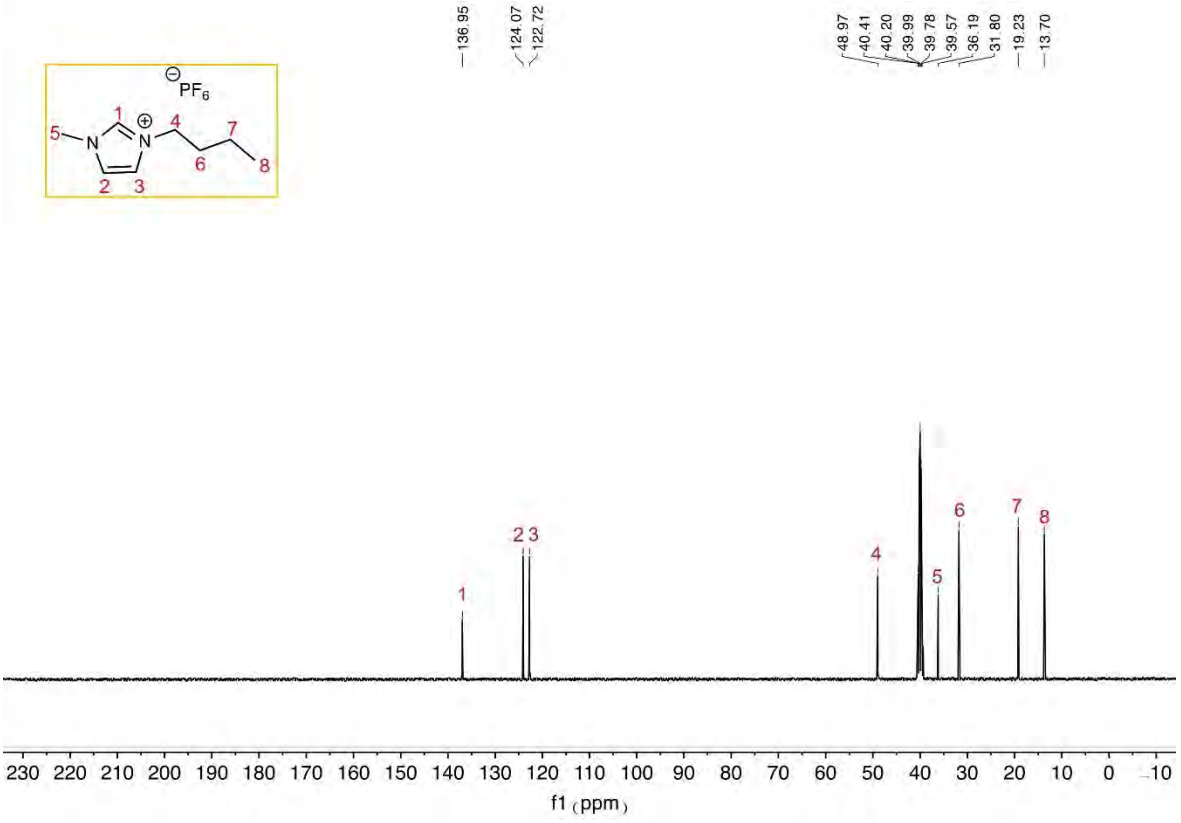

Figure S3. 13C NMR of [BMIM]PF_6.

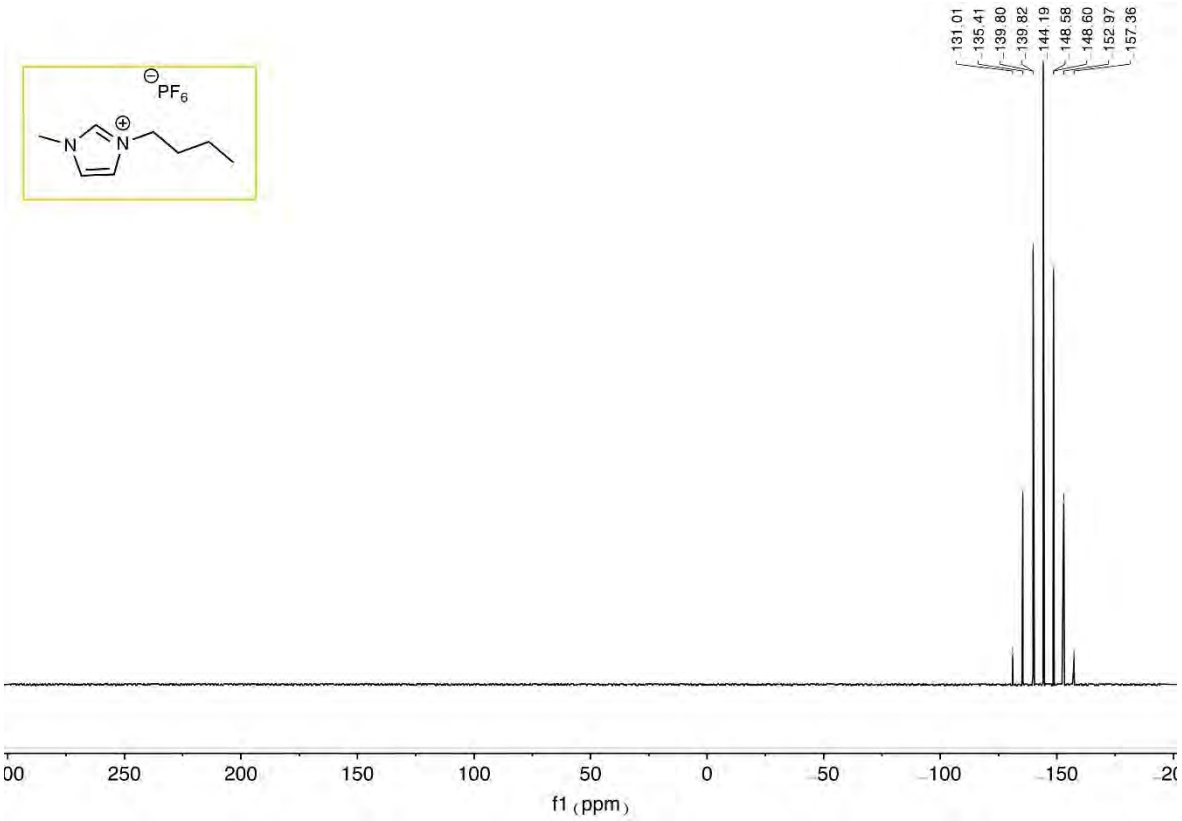

Figure S4. 31P NMR spectra of [BMIM]PF_6.

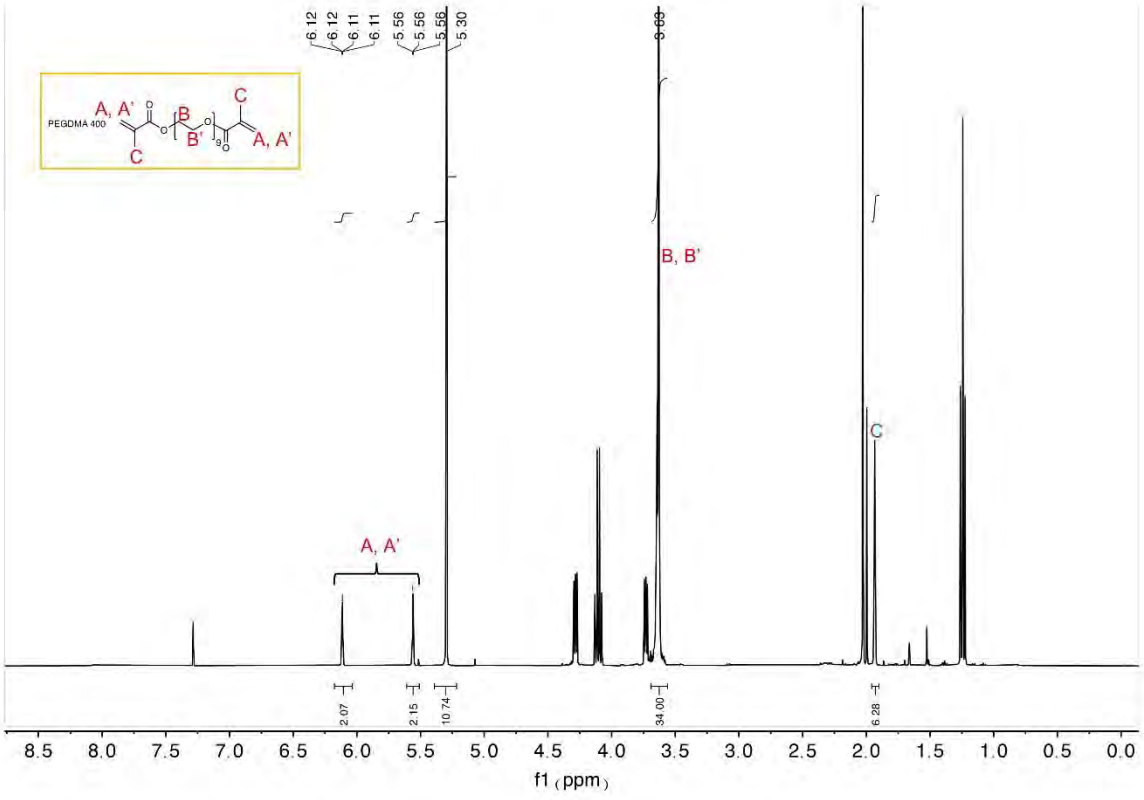

Figure S5. 1H NMR spectra of PEGDMA made from PEG 400.

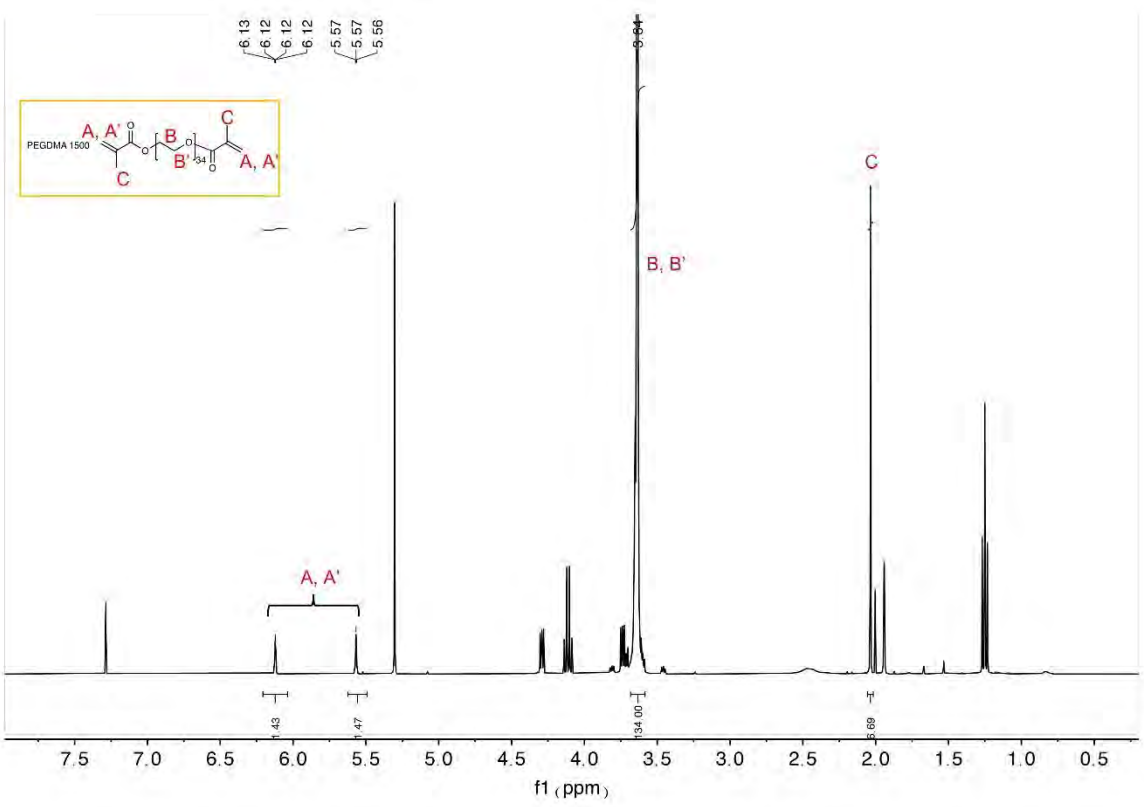

Figure S6. 1H NMR spectra of PEGDMA made from PEG 1500.

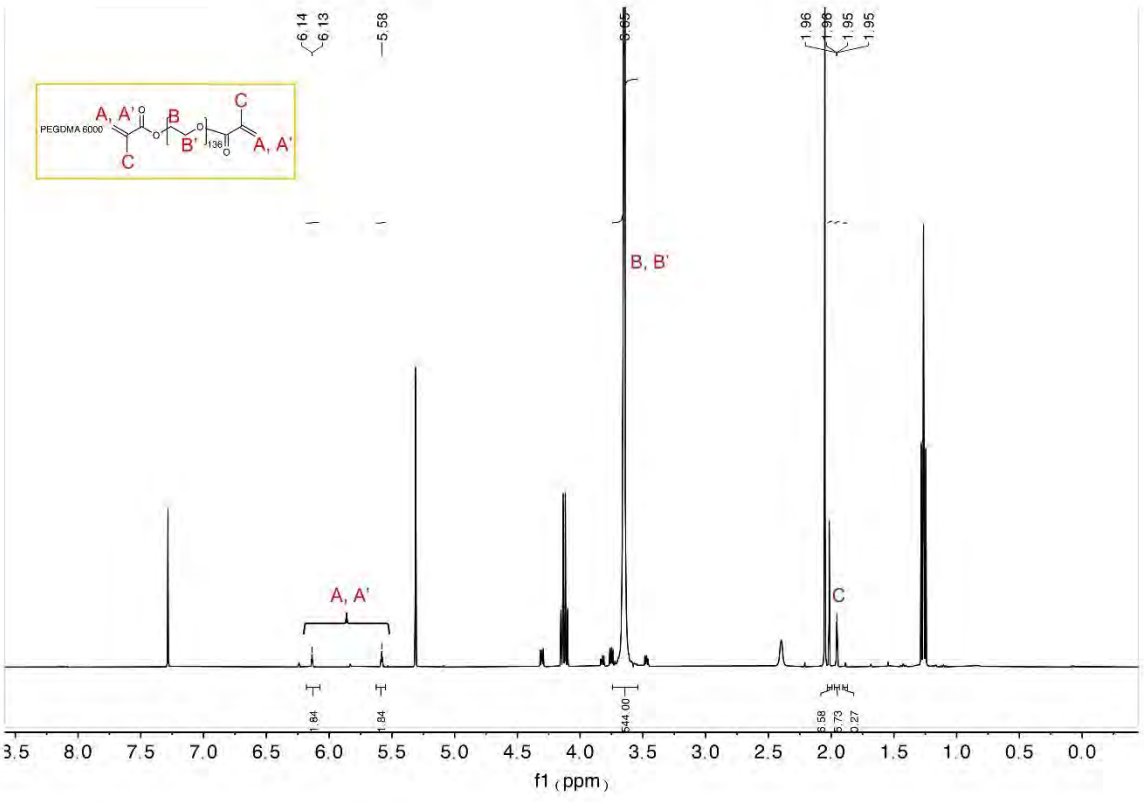

Figure S7. 1H NMR spectra of PEGDMA made from PEG 6000.

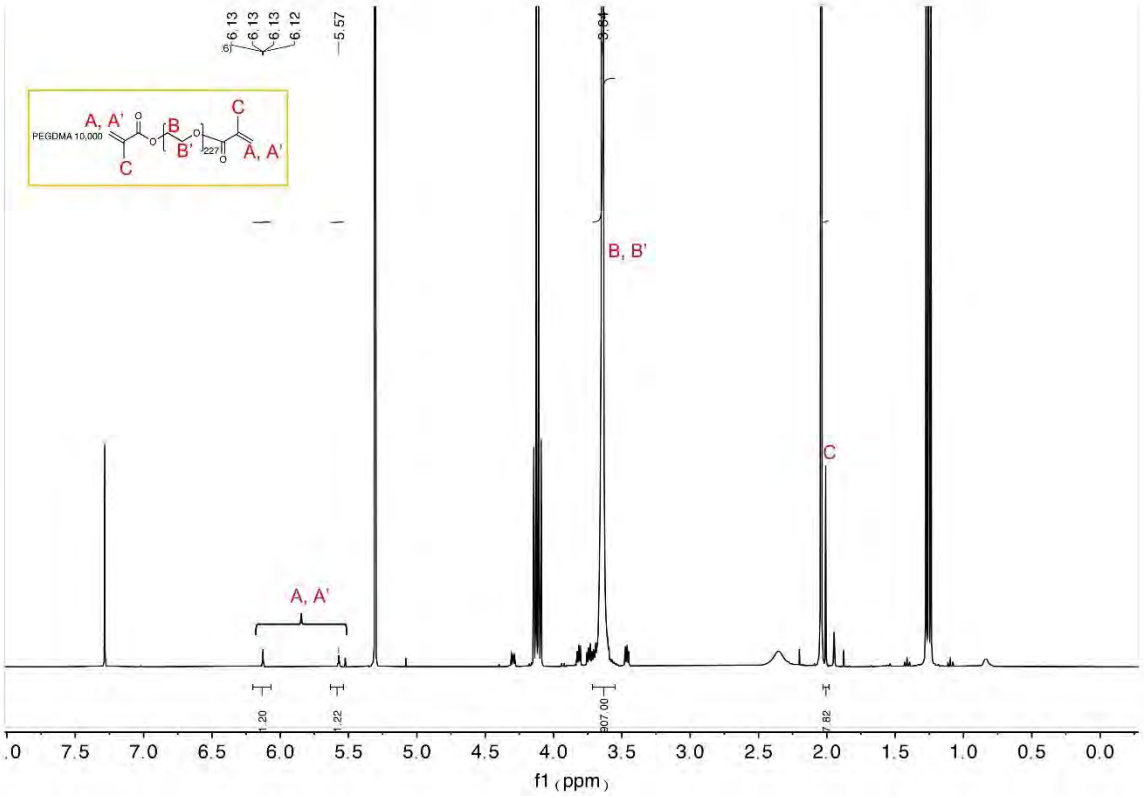

Figure S8. 1H NMR spectra of PEGDMA made from PEG 10000.

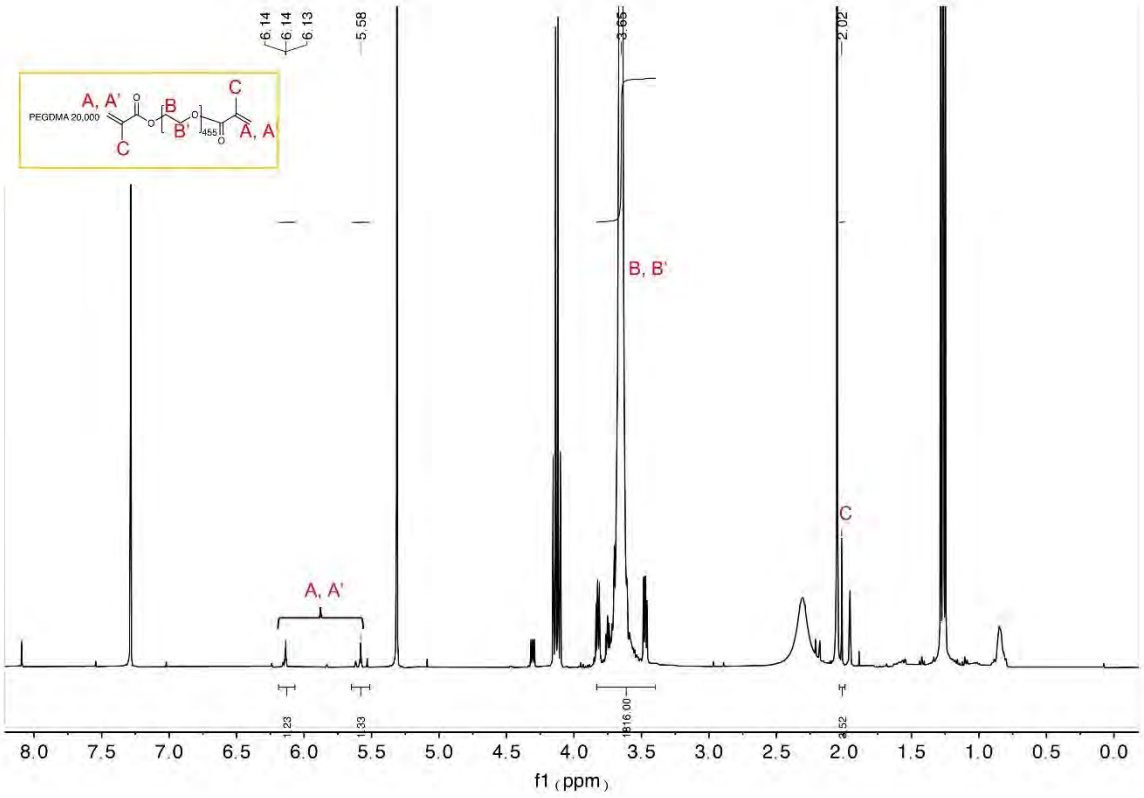

Figure S9. 1H NMR spectra of PEGDMA made from PEG 20000.

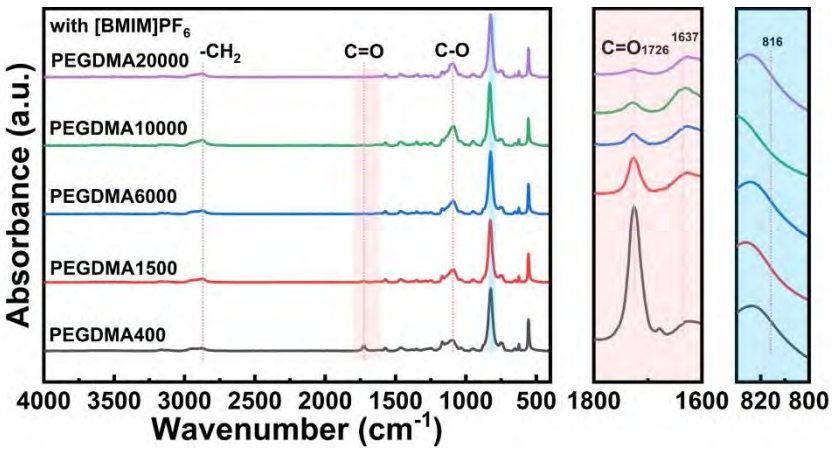

Figure S10. Cross-link density of PEG with different molecular masses.

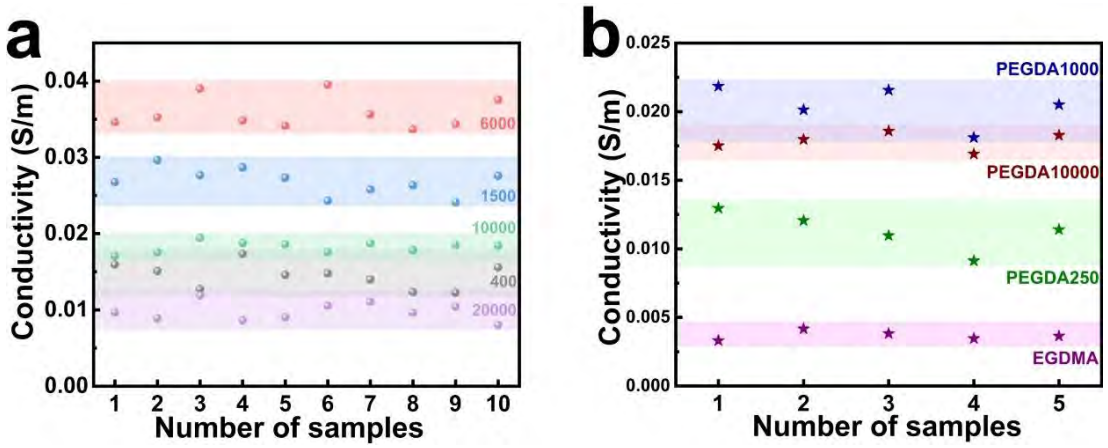

Figure S11. Conductivity of the ionogels synthesized from a) PEGDMA and b) EGDMA and PEGDA.

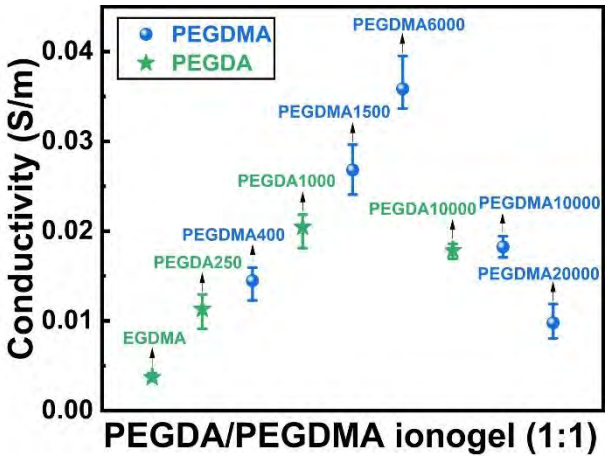

Figure S12. Dependence of the cross-link density on the conductivity of the PEGDA and PEGDMA ionogels (cross linker:[BMIM]PF_6=1:1).

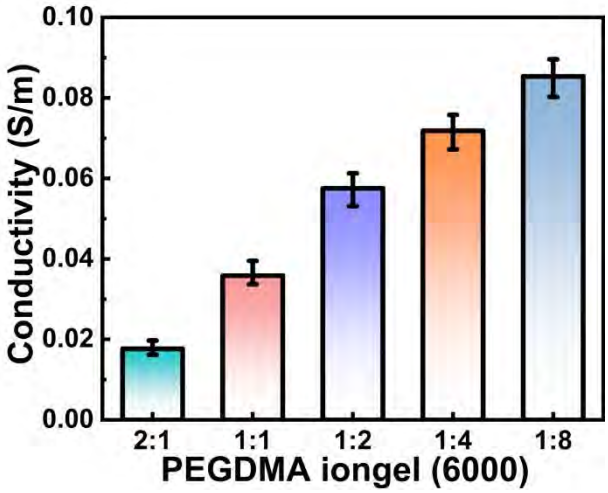

Figure S13. Conductivity of the ionogels with different ionic liquid concentrations.

As shown in the Figure 2g and Figure S14, with the increase of PEGDMA:[BMIM]PF_6 ratio from 1:2 to 1:8, obvious decrease trends were observed in strength at break, elongation at break, as well as Young's modulus. Therefore, excess ILs will conversely reduce the mechanical properties of ionogels.

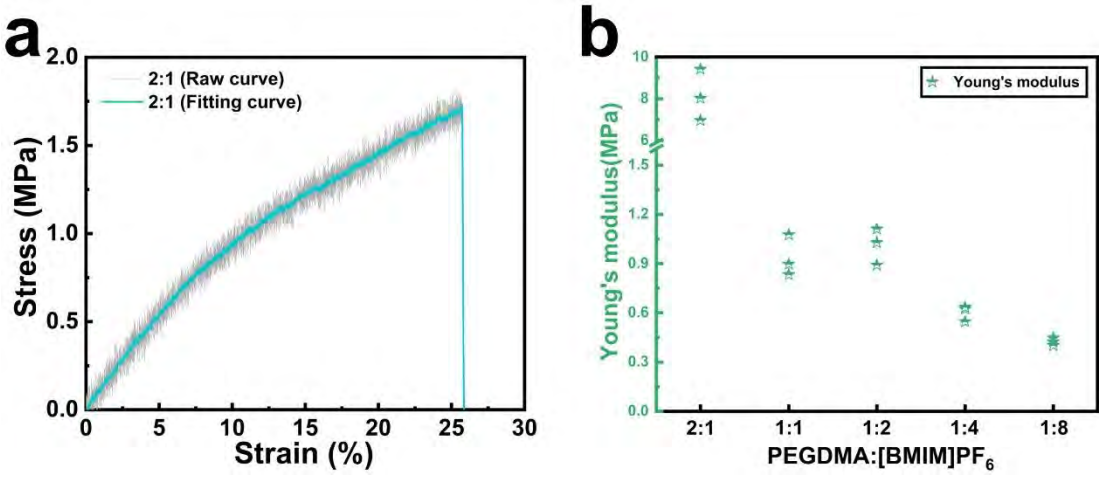

Figure S14. a) Strain-stress curve of ionogel with PEGDMA:[BMIM]PF_6=2:1, and b) Young's modulus of ionogels with different PEGDMA:[BMIM]PF_6 ratios.

As shown in Figure S12, when a droplet drips and spreads on the TENG, the accumulated negative charges (due to previous droplets) on the top surface, attract the positive charges inside the droplet to build a charge balance at the liquid-solid interface. As soon as the droplet touches the top-electrode, directional and rapid charge transfer happens between electrodes to

neutralize the induced positive charges in the droplet, leading to a sharp current peak. With the sliding of the droplet, electrons generally flow back to get a final balance between the electrodes, and thus form an opposite current. Since the "contacting" process of a droplet takes much less time than its "sliding" process, the opposite signal is usually much wider but shorter. After the droplet leaves the device, there will be no charge difference between the electrodes but only the accumulated negative charges left on the top surface waiting for the next droplet.

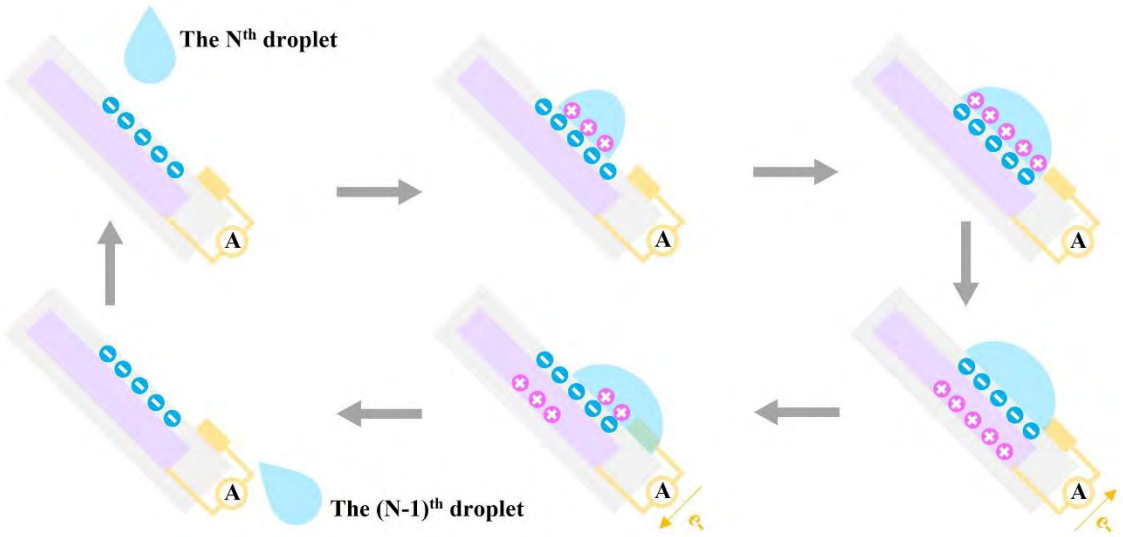

Figure S15. Working principle of I-TENGs for water droplets energy harvesting.

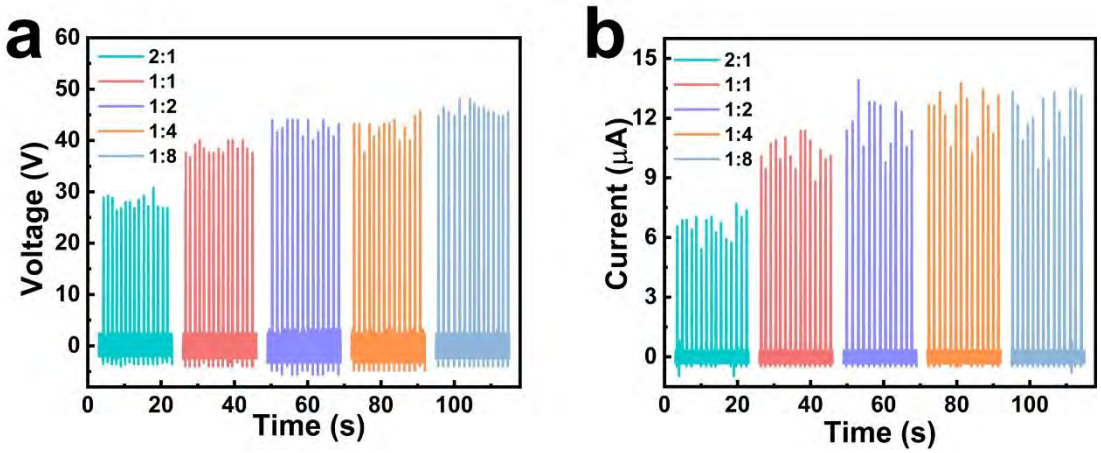

Figure S16. Effect of ionic liquid concentration on the device output: a)voltage and b) current.

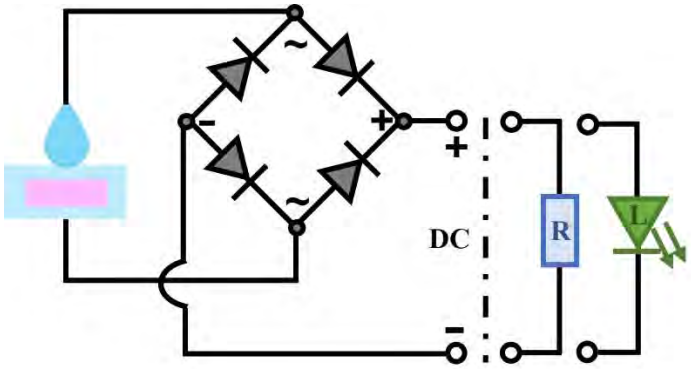

Figure S17. Schematic diagram of rectified circuit connected with external load such as resistors and LEDs.

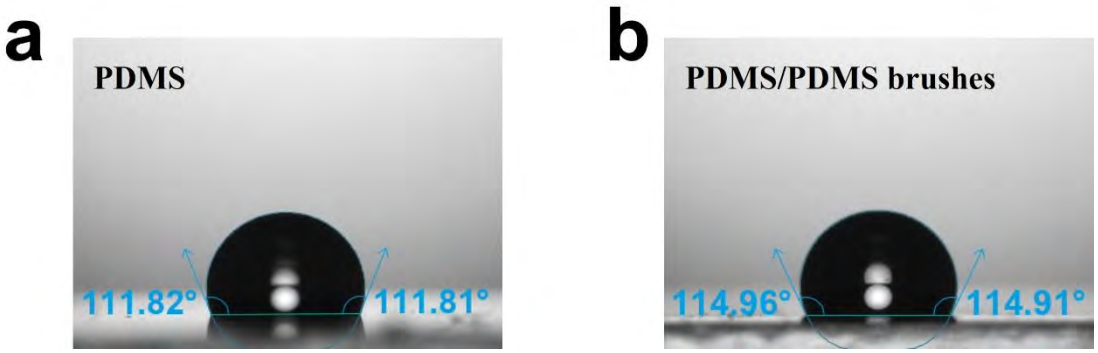

Figure S18. Water contact angle of a) the untreated PDMS film and b) PDMS/PDMS brushes film.

As shown in Figure S19, no apparent difference was observed in scanning electron microscopy (SEM) images for PDMS films with or without PDMS brushes. With further investigation on PDMS film by atomic force microscopy (AFM), it was found in Figure S20 that the PDMS films without or with PDMS brushes show obvious surface differences, which is consistent with previous report[S1] and indicates the successful growth of PDMS brushes on PDMS surface.

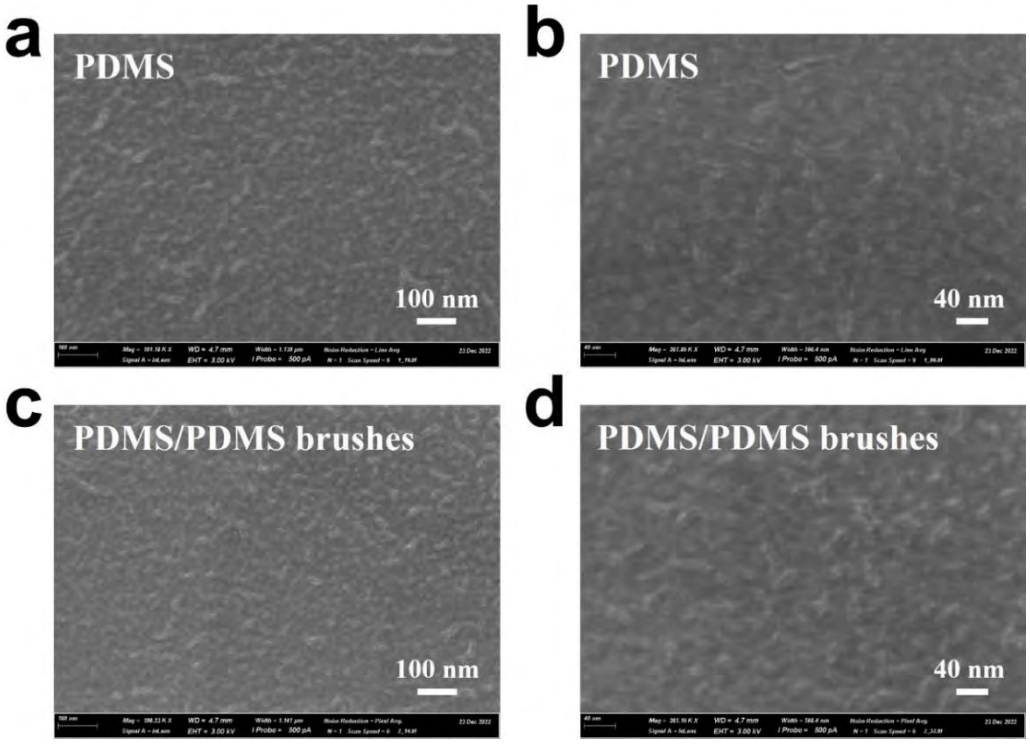

Figure S19. SEM images a,b) the untreated PDMS film and c,d) PDMS/PDMS brushes film.

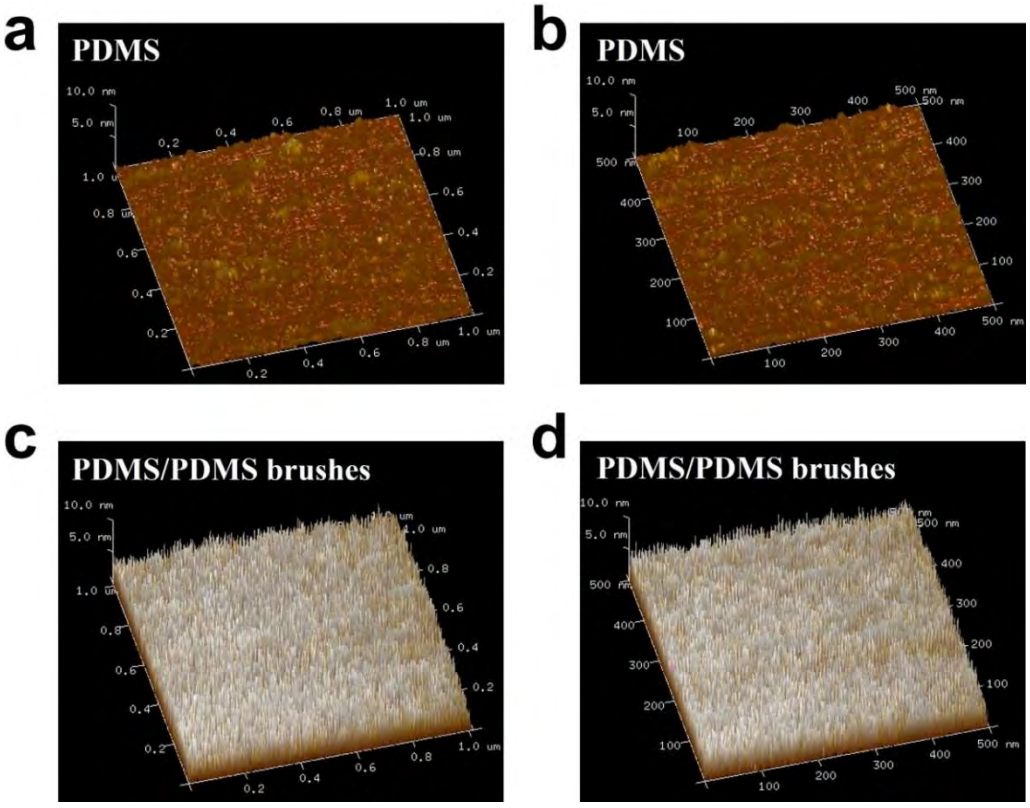

Figure S20. AFM images a,b) the untreated PDMS film and c,d) PDMS/PDMS brushes film.

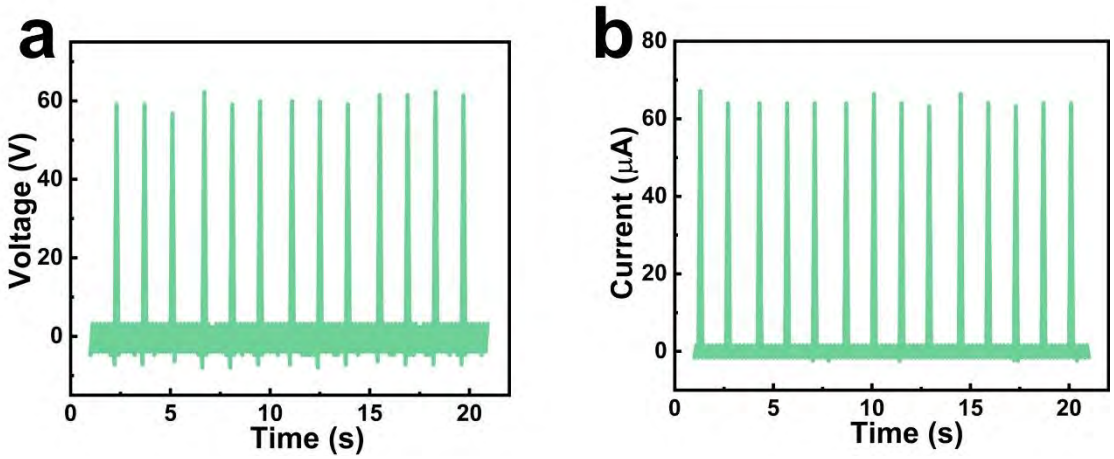

Figure S21. a) voltage and b) current signals of PI-TENG by dripping a single droplet from rainwater.

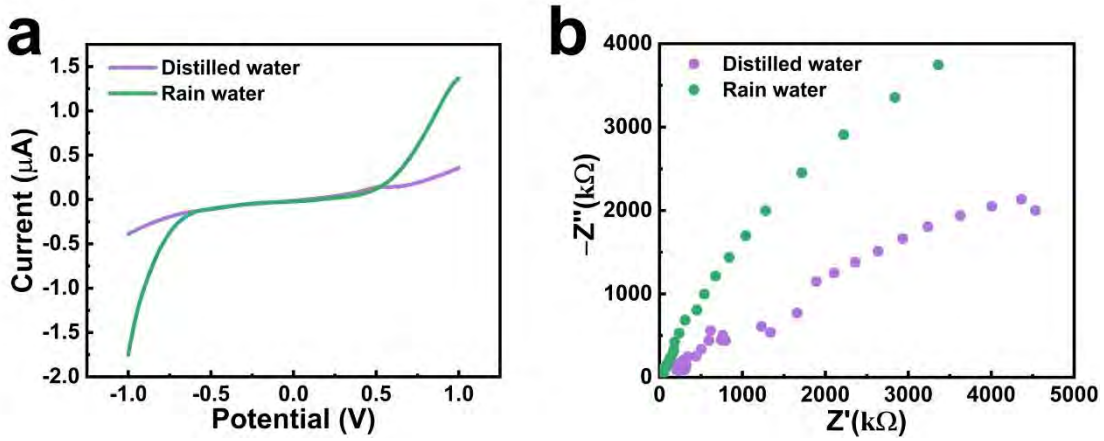

Figure S22. a) LSV and b) EIS curves of the distilled water and rainwater collected in Zurich.

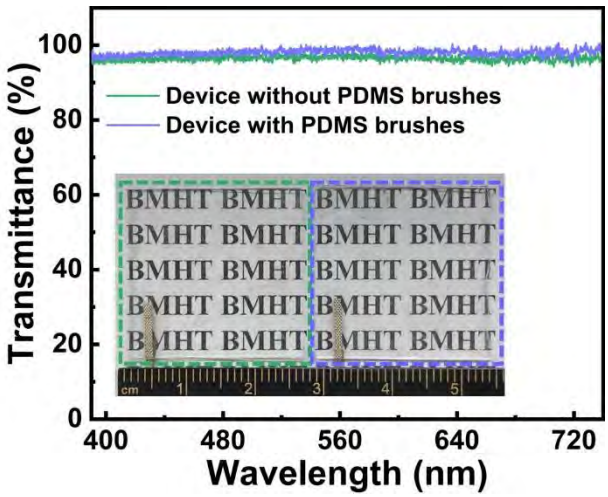

Figure S23. Transmittance of the I-TENGs without or with PDMS brushes, inset is the photograph of these two devices.

Table S1. Output performance comparison with common TENGs in droplet energy harvesting.

Ref.	Device structure	Droplet Type	Droplet volume	Voltage (V)	Current (μA)	Power (μW)
[S2]	Leaf blade /petiole	0.1M NaCl	33 μL	1.3	4.1 (rain 1μA)	1
[S3]	Ag/PDMS/Ag/Si /Al	Rainwater	20 μL	~38	~11	183
[S4]	HDL/ITO/PDMS/VHB	DI water Tap water	110 μL	~62 ~59	/	21.5 (215 mW/m^2)
[S5]	PTFE/Cu/Kapton	Rainwater	(22 mL/s)	28.9	9.1	/
[S6]	EVA/CF/MF /rubber	Rainwater	120 μL	~0.42	~0.03	/
[S7]	PTFE/Ag/Nylon	DI water/Rainwater Tap water/0.6M NaCl	40 μL	5.2/4.6 3.0/1.6	0.53/0.42 0.24/0.16	22.1/12.6 7.1/3.2
[S8]	Parylene/Ni	Rainwater/Tap water DI water	/	0.3/0.5 3.3	1.5/1.5 0.6	/
[S9]	PTFE/C-textile	DI water 0.015M/0.6M NaCl	50 μL	60 50/38	9 /	/
[S10]	Al/PTFE	Tap water 0.1M NaCl	100 μL	~60 ~30	/	/
[S11]	PTFE/C-fiber	Rainwater	/	~12	~0.8	/
This work	Ionogel/PDMS/PDMS brushes	Distilled water rainwater	12.5 μL	55.4 60.4	14.6 60	213.3 687.5

(Note: here we only summarized droplet-TENGs that have provided the droplet type information, as the droplet type is one of the key factors that affects the output performance of droplet-TENG.)

Table S2. Summary of the photovoltaic parameters of commercial solar cell (SC), SC+I-TENG, and SC+PI-TENG.

Samples	J_{SC} (mA/cm^2)	V_{OC} (V)	FF	PCE (%)
SC	5.81±0.07	3.44±0.01	0.852±0.025	17.14±0.46
SC+I-TENG	5.88±0.07	3.45±0.02	0.849±0.023	17.23±0.53
SC+PI-TENG	6.13±0.14	3.46±0.02	0.853±0.026	18.24±0.36

Table S3. Comparison of the effect of TENG on PCE of SC with reported works.

Ref.	TENG	Solar cell (SC)	Effect of TENG on PCE of SC
[S12]	ITO/MNS-PDMS	+Al/P3HT:$PC_{60}BM$/MoO_3	Increase from 2.89% to 3.29%
[S13]	ITO/PDMS	Commercial SC	Decrease from 18.9% to 18.4%
[S14]	PVA-PEI-CDs/FEP	Commercial Si-SC	Increase from 13.6% to 14.6%
[S15]	Ag-ITO/NW-PDMS	+Si absorption layer/Al	Increase from 12.55% to 13.57%

[S16]	PET/ITO/PTFE	Si-based SC	Decrease from 16% to 14%
[S17]	ITO/PDMS-ITO/SiN	Si micropyramid SC	Decrease from 16% to 14%
[S18]	ITO/ZnO NWs-PDMS/ITO	DSSC	Decrease from 7.36% to 6.06%
[S19]	Ag-ITO/SiO_2	+Si absorption layer/Al	Increase from 15.17% to 15.71%
This work	Ionogel/PDMS/PDMS brushes	Commercial Si-SC	Increase from 17.14% to 18.24%

3. Reference

[S1] S. Li, Y. Hou, M. Kappl, W. Steffen, J. Liu, H-J. Butt, *Adv. Mater.* **2022**, *34*, 2203242.

[S2] H. Wu, Z. Chen, G. Xu, J. Xu, Z. Wang, Y. Zi, *ACS Appl. Mater. Interfa*ces **2020**, *12*, 56060–56067.

[S3] L. Zhao, J. Duan, L. Liu, J. Wang, Y. Duan, L. Vaillant-Roca, X. Yang, Q. Tang, *Nano Energy* **2021**, *82*, 105773.

[S4] J. Wang, L. Ma, J. He, Y. Yao, X. Zhu, L. Peng, J. Yang, K. Li, M. Qu, *Chem. Eng. J.* **2022**, *431*, 134002.

[S5] X. Liu, A. Yu, A. Qin, J. Zhai, *Adv. Mater. Technol.* **2019**, *4*, 1900608.

[S6] Y-C. Lai, Y-C. Hisao, H-M. Wu, Z. L. Wang, *Adv. Sci.* **2019**, *6*, 1801883.

[S7] L. Zhao, L. Liu, X. Yang, H. Hong, Q. Yang, J. Wang, Q. Tang, *J. Mater. Chem. A* **2020**, *8*, 7880–7888.

[S8] X. Gang, Z. H. Guo, Z. Cong, J. Wang, C. Chang, C. Pan, X. Pu, Z. L. Wang, *ACS Appl. Mater. Interfa*ces **2021**, *13*, 20145–20152.

[S9] F. Liang, X. Chao, S. Yu, Y. Gu, X. Zhang, X. Wei, J. Fan, X. Tao, D. Shou, *Adv. Energy Mater.* **2022**, *12*, 2102991.

[S10] N. Zhang, H. Gu, K. Lu, S. Ye, W. Xu, H. Zheng, Y. Song, C. Liu, J. Jiao, Z. Wang, X. Zhou, *Nano Energy* **2021**, *82*, 105735.

[S11] W. Yuan, C. Zhang, B. Zhang, X. Wei, O. Yang, Y. Liu, L. He, S. Cui, J. Wang, Z. L. Wang, *Adv. Mater. Technol.* **2021**, 2101139.

[S12] Z. Ren, Q. Zheng, H. Wang, H. Guo, L. Miao, J. Wan, X. Chen, S. Cheng, H. Zhang, *Nano Energy* **2020**, *67*, 104243.

[S13] D. Yang, Y. Ni, H. Su, Y. Shi, Q. Liu, X. Chen, D. He, *Nano Energy* **2020**, *79*, 105394.

[S14] L. Wang, Y. Wang, H. Wang, G. Xu, A. Döring, W. A. Daoud, J. Xu, A. L. Rogach, Y. Xi, Y. Zi, *ACS Nano* **2020**, *14*, 10359−10369.

[S15] X. Liu, K. Cheng, P. Cui, H. Qi, H. Qin, G. Gu, W. Shang, S. Wang, G. Cheng, Z. Du, *Nano Energy* **2019**, *66*, 104188.

[S16] L. Zheng, Z-H. Lin, G. Cheng, W. Wu, X. Wen, S. Lee, Z. L. Wang, *Nano Energy* **2014**, *9*, 291−300.

[S17] Y. Yang, H. Zhang, Y. Liu, Z-H. Lin, S. Lee, Z. Lin, C. P. Wong, Z. L. Wang, *ACS Nano* **2013**, *7*, 2808−2813.

[S18] B. Dudem, Y. H. Ko, J. W. Leem, J. H. Lim, J. S. Yu, *ACS Appl. Mater. Infterces* **2016**, *8*, 30165−30175.

[S19] X. Liu, P. Cui, J. Wang, W. Shang, S. Zhang, J. Guo, G. Gu, B. Zhang, G. Cheng, Z. Du, *Nanotechnology* **2021**, *32*, 075401.